A hypothalamic novelty signal modulates hippocampal memory

Shuo Chen, Linmeng He, Arthur J y Huang, Roman Boehringer, Vincent Robert, Marie Wintzer, Denis Polygalov, Adam Z Weitemier, Yanqiu Tao, Mingxiao Gu, et al.

A hypothalamic novelty signal modulates hippocampal memory

Shuo Chen[1]*, Linmeng He[1,2], Arthur J.Y. Huang[1], Roman Boehringer[1], Vincent Robert[3], Marie E. Wintzer[1], Denis Polygalov[1], Adam Z. Weitemier[1], Yanqiu Tao[1], Mingxiao Gu[1], Steven J. Middleton[1], Kana Namiki[4], Hiroshi Hama[4], Ludivine Therreau[3], Vivien Chevaleyre[3,5], Hiroyuki Hioki[6], Atsushi Miyawaki[4,7], Rebecca A. Piskorowski[3,5], Thomas J. McHugh[1,2]*

[1]Laboratory for Circuit and Behavioral Physiology, RIKEN Center for Brain Science, Wakoshi, Saitama, Japan.

[2]Department of Life Sciences, Graduate School of Arts and Sciences, The University of Tokyo, Tokyo, Japan.

[3]Université de Paris, Institute of Psychiatry and Neuroscience of Paris INSERM UMRS1266, 102-015 rue de la santé, 75014 Paris France.

[4]Laboratory for Cell Function and Dynamics, RIKEN Center for Brain Science, Wakoshi, Saitama, Japan.

[5]GHU PARIS Psychiatry and Neuroscience, 75014 Paris, France.

[6]Department of Cell Biology and Neuroscience, Juntendo University Graduate School of Medicine, Tokyo, Japan.

[7]Biotechnological Optics Research Team, RIKEN Center for Advanced Photonics, Wakoshi, Saitama, Japan.

*Corresponding author. E-mail: shuoshu@gmail.com (S.C.), thomas.mchugh@riken.jp (T.J.M.)

The ability to recognize information incongruous with previous experience is critical for survival, thus novelty signals in the mammalian brain have evolved to enhance attention, perception and memory[1-3]. Although the importance of regions such as the ventral tegmental area[4-6] and locus coeruleus[6,7] in broadly signaling novelty has been well established, these diffuse monoaminergic transmitters have yet to be shown to convey specific information regarding the type of stimuli that drive them[6]. Whether distinct types of novelty, such as contextual and social novelty, are differently processed and routed in the brain remain unclear. Here we identify a novelty hub in the hypothalamus – the supramammillary nucleus (SuM)[8]. Unique about this region is that it not only responds broadly to novel stimuli, but segregates and selectively routes different types of information to discrete cortical targets, the dentate gyrus (DG) and CA2 fields of the hippocampus, for the modulation of mnemonic processing. Taking advantage of a novel SuM-Cre transgenic mouse, we found that DG-projecting SuM neurons are activated by contextual novelty while the SuM-CA2 circuit is preferentially activated by novel social encounters. Circuit-based manipulation demonstrated that divergent novelty channeling in these projections significantly modifies hippocampal-based contextual or social memory. This content-

specific routing of novelty signals represents a previously unknown mechanism that enables the hypothalamus to flexibly modulate select components of cognition.

The hypothalamus supports evolutionary conserved functions, including the regulation of homeostatic states and innate behaviors[9]. However, given both the conservation of a behavioral novelty response across species and the hypothalamic connections with the hippocampus, this region may play a role in detecting novelty and influencing higher cognitive processing. Thus, we conducted a systematic examination of the expression of c-Fos, a marker of active neurons, in the hypothalamus of mice exposed to two omnipresent types of novelty, contextual and social (Fig. 1a). While c-Fos expression increased in multiple hypothalamic regions, the SuM, a small nucleus with direct projections to hippocampus[8], exhibited a remarkably high response to both contextual[10,11] and social novelty (Fig. 1b and Extended Data Fig. 1), with similar proportions of neurons activated in both conditions (Fig. 1c, novel context: 117.9 ± 4.1 c-Fos+ cells/mm^2; novel animal: 129.9 ± 5.4; familiar context (control): 24.0 ± 2.5). To physiologically characterize the novelty response of SuM neurons, we performed *in vivo* single-unit recordings in behaving mice (Fig. 1d, e and Extended Data Fig. 2a–c). Each session consisted of exposure to a familiar context, a novel context and finally a novel animal (Fig. 1d). A total of 141 well-isolated units were recorded, comprised of 119 putative excitatory neurons (pEN, 84.4%) and 22 putative fast-spiking interneurons (pIN, 15.6%). The average firing rate of all pEN units was significantly higher during exposure to a novel context (2.5 Hz) or a novel social encounter (2.6 Hz) compared to familiar contexts (2.1 Hz; Fig. 1f, g), whereas pIN units showed no significant novelty modulation (Extended Data Fig. 2d–h). Subsets of pEN units significantly increased their activity in response to contextual novelty (21.8%, 26 of 119 units) and social novelty (21.0%, 25 of 119 units), outweighing the subsets that showed decreased firing rates (8.4%, 10 of 119 units for contextual; 0.8%, 1 of 119 units for social; Fig. 1h, i). Notably, a large portion of SuM neurons (69.2%, 27 of 39 units) were specifically excited by one type of novelty but inhibited or non-responsive to the other (Fig. 1f, j). Both the context and social driven populations displayed a monotonic decrease in firing rates over time (Fig. 1k), suggesting uniform habituation of the novelty response.

The SuM and related circuits have been difficult to study due to their small size and diverse cell types[8]. Therefore, we developed a novel transgenic mouse line, Csf2rb2-Cre, to gain precise

genetic access to the SuM (SuM-Cre mouse; Fig. 2 and Extended Data Fig. 3). The pattern of Cre expression in this line, confirmed by crossing with a β-gal Cre reporter line[12] (Extended Data Fig. 3c, d), recapitulated the endogenous Csf2rb2 pattern[13], with robust expression in neurons of the SuM. Injection of Cre-dependent adeno-associated virus (AAV) vector expressing eYFP into the SuM resulted in a SuM-restricted signal (Fig. 2a, b) and strong terminal labeling in the pyramidal layer of CA2 and the granule cell layer of the DG in the hippocampus[8] (Fig. 2a, c and Extended Data Fig. 4). We further used tissue clearing techniques (Sca*l*eS)[14] to image SuM projections in the whole brain and observed axons extending through the fornix superior and the fimbria to a wide dorsal-ventral range of DG and CA2 (Extended Data Fig. 5).

To ask if these pathways are anatomically segregated, we simultaneously injected Cre-dependent retrograde AAVs expressing eYFP and mCherry into the DG and CA2 of single mice (Fig. 2d, e and Extended Data Fig. 6a). The majority of the identified SuM neurons were found to project solely either to the DG (37.3 ± 2.2%, $N = 6$ mice, $n = 2{,}700$ neurons) or CA2 (39.4 ± 3.8%, $N = 6$ mice, $n = 2{,}700$ neurons) with less than a quarter (23.3 ± 2.7%, $N = 6$ mice, $n = 2{,}700$ neurons) dually infected (Fig. 2e). The high viral titer and proximity of the CA2 and DG injection sites raised the possibility that the dually infected population could be overestimated; thus we injected small volumes of Alexa Fluor 488 and Alexa Fluor 594 cholera toxin subunit B (CTB) into the DG and CA2, respectively, and found a very small fraction of doubly labeled neurons[15] (2.6 ± 0.5%, $N = 3$ mice, $n = 708$ neurons, Extended Data Fig. 6b). Further, single injections of retrograde AAV into CA2 or DG revealed robust fibers only in the injection region, with no collaterals or synaptic transmission detected in the other (Extended Data Fig. 7a–d), confirming that these pathways are largely segregated.

We next asked if novelty-driven SuM neurons project to hippocampus and whether novelty information with distinct features, e.g. contextual and social, is differentially routed. We bred the SuM-Cre mice with the Tet-Tag mouse line[16], carrying the c-Fos-tTA transgene to permit long-term tagging of c-Fos activity in the SuM (Fig. 3a–d). These mice allowed dual-color labeling of temporally segregated active SuM ensembles, visualized by c-Fos-triggered viral eYFP expression (green) and anti-c-Fos immunohistochemistry (red), respectively. Consistent with our electrophysiological results, sequential presentation of two different types of novelty revealed significant segregation of active ensembles (Fig. 3c, d). For simultaneous circuit tracing and c-

Fos labeling, we injected retrograde AAVs expressing mCherry either into the DG or CA2 and AAV-TRE-DIO-eYFP into the SuM of the double-transgenic mice (Fig. 3e–j). Significantly higher c-Fos activity was observed in the DG-projecting population compared to the CA2-projecting population in mice exposed to contextual novelty (Fig. 3j, DG-projecting: 39.2 ± 1.8% versus CA2-projecting: 16.3 ± 1.1%). In contrast, in mice exposed to a novel social stimulus, c-Fos expression was significantly elevated in the CA2-projecting neurons compared to the DG-projecting ones (Fig. 3j, CA2-projecting: 32.8 ± 2.2% versus DG-projecting: 12.4 ± 1.1%). Similar results were observed when anti-c-Fos immunohistochemistry was used to assay activity in SuM-Cre mice injected with retrograde AAVs either into the DG or CA2 for circuit labeling (Extended Data Fig. 8a–f).

To validate this novelty-specific projection bias, we conducted *in vivo* single unit recordings in the SuM (Fig. 3k–t). Single-unit activity was recorded in the SuM during low-frequency laser stimulation to induce antidromic spikes in mice with ChR2 expression in the SuM and optic fibers above DG and CA2 (Fig. 3l–q and Extended Data Fig. 8g–l), permitting projection-specific optogenetic identification of SuM neurons. The majority of the DG-projecting neurons (10 of 12 units) increased their firing rate in a novel context (Fig. 3r, example cells 1 and 2) and the average firing rate change across the population was higher with novel contextual exposure than during novel social exposure (Fig. 3s, contextual: 0.39 versus social: 0.13). In contrast, most CA2-projecting neurons (15 of 17 units) exhibited a larger firing rate increase in response to social novelty than to contextual novelty (Fig. 3r, example cells 3 and 4; Fig. 3t, social: 0.43 versus contextual: 0.18).

The novelty-selective activation of the SuM-DG and SuM-CA2 circuits led us to assess whether manipulation of either circuit impacts hippocampal memory in a feature (contextual or social)-dependent way. We employed optogenetics to dissect the two circuits by delivering light to axon terminals in either the DG or CA2 (Fig. 4; Extended Data Fig. 7). Contextual behavior was assessed using a one-day habituation protocol in a novel high-walled enclosure (Fig. 4a and Extended Data Fig. 9). Following three habituation sessions (A1–A3), across which all groups decreased exploration (Fig. 4b–e) indicating familiarization to the environment[17], light was delivered to SuM terminals in the hippocampus (Session A4 in Fig. 4a). Only mice in which the SuM-DG pathway was activated altered their behavior, increasing exploration compared to the

controls (Fig. 4b, relative travel distance: 58.1 ± 3.4% versus 39.6 ± 5.6%), consistent with an increased perception of contextual novelty. We then altered the now familiar context by displacing the local objects and changing the visual cues on the walls (Session B1 in Fig. 4a, Extended Data Fig. 9a). Control mice reacted to this contextual novelty by increasing their exploration during the session, however this response was absent in mice in which the SuM terminals in the DG were inhibited (Fig. 4c, relative traveling distance: DG/eNpHR: 38.1 ± 4.6% versus DG/EYFP: 71.6 ± 3.8%), suggesting a deficiency in contextual novelty recognition. A final session (B2) in the altered context in the absence of light confirmed that once relieved from SuM-DG inhibition the mice could recognize the contextual change (Fig. 4c). Identical sets of experiments were performed with ChR2- or eNpHR-transfected mice in the absence of light delivery and no changes were found in behavior (Extended Data Fig. 9f–i). These results demonstrate that the novelty signal routed by the SuM to DG projection can modulate behavior based on hippocampal contextual memory.

Next we employed a direct interaction test to explore the impact of SuM inputs on social memory (Fig. 4f–k). Subject mice were first exposed to a novel mouse without light stimulation and interaction time was scored. One hour later mice were either re-exposed to the same mouse or exposed to a second novel mouse, with light delivered to the DG or CA2. In CA2-targeted mice we found that photostimulation caused a deficit in the expression of social memory, as these mice exhibited high levels of social interaction, resulting in a significantly higher habituation index compared to the controls (Fig. 4h, CA2/ChR2: 0.116 ± 0.081 versus CA2/eYFP: −0.373 ± 0.103). Optogenetic manipulations targeting the DG, regardless of stimulation or inhibition, showed no effect on social interaction (Fig. 4g, j). These data suggest that the SuM to CA2 pathway can drive social novelty-linked exploratory behavior and routes social instead of contextual novelty to the hippocampus.

To understand how these projections influence the hippocampus we examined how the two discrete SuM-hippocampal circuits differ in neurotransmission (Extended Data Figs. 6c–h and 10). Multiplex fluorescence *in situ* hybridization (RNAscope, Extended Data Fig. 6c–h) in mice injected with retrograde AAVs expressing eYFP into the DG or CA2 found that while Cre recombination occurs in both glutamatergic and GABAergic neurons, the majority of DG-projecting neurons are positive for both VGLUT2 and VGAT[15,18,19], whereas most CA2-

projecting neurons are only VGLUT2+. Consistent with this, whole cell voltage-clamp recordings in acute hippocampal slices (Extended Data Fig. 10) revealed DG-projecting SuM neurons simultaneously release both glutamate and GABA (Extended Data Fig. 10f–j)[15,18,19], while SuM-CA2 transmission is entirely glutamatergic (Extended Data Fig. 10k–o). While both inputs induced modest excitatory post-synaptic currents (EPSCs) in their target hippocampal principal neurons, they shared a robust feed-forward inhibitory component, evidenced by the large inhibitory post-synaptic currents (IPSCs) seen in DG granule cells (GCs) or CA2 pyramidal neurons (PNs) upon SuM axon stimulation. This regulation of the local excitation/inhibition (E/I) balance in the hippocampus has been speculated to contribute to the fine tuning of neuronal excitability and the dynamic range of neuroplasticity during mnemonic processing[19-21]. Thus, SuM transmission may provide an alternative and highly flexible mode of novelty signaling for shaping hippocampal encoding, in complement to the modulatory effects of monoaminergic innervation.

To better understand how the wide anatomical connectivity[8] of the SuM underlies this signaling we used projection-specific tracing to profile upstream inputs to the DG- and CA2-innervating SuM neurons (Extended Data Fig. 11). Both populations receive extensive inputs from subcortical regions, and although there were no significant statistical differences, inputs to the DG-projecting population were skewed towards brain regions in the reward and motor systems, while the CA2 projectors received proportionally more inputs from neurons in socially engaged regions, particularly the paraventricular hypothalamic nucleus[22] and medial preoptic area[23] (Extended Data Fig. 11g, h). This projection-specific connectivity may underlie the ability of the SuM to segregate contextual and novelty signals. In contrast to these diverse inputs, the ascending outputs of the hippocampal projecting SuM neurons are fairly restricted to the hippocampus (Extended Data Figs. 4 and 5). Therefore, the SuM may integrate internal states with cognitive input, extracting the contextual and social salience of stimuli and routing this signal for the modulation of mnemonic processing.

The observed selectivity of the SuM-DG and SuM-CA2 circuits supports the idea of specialized information processing along the longitudinal axis of the hippocampus[24]. The DG[25-27] can rapidly detect and encode contextual changes, while the loss of synaptic plasticity in DG GCs impairs context discrimination and novelty recognition[28,29] but not social memory[30]. Therefore,

182 the SuM input to DG GCs, via regulation of local E/I balance, may serve as a key facilitator of
183 plasticity at the perforant pathway when new contextual information is encoded[19]. In contrast,
184 interventions targeting pyramidal cells in CA2 have no impact on contextual learning, but rather
185 result in profound changes in social memory[31-36]. We found that activation of the SuM input in
186 CA2, which engages strong feed-forward inhibition (Extended Data Figs. 10), could induce a
187 social novelty response (Fig. 4h), however inhibition could not impair an endogenous response
188 (Fig. 4k), suggesting redundancy in this circuitry. We speculate that the SuM inputs to dorsal
189 CA2 may shift local E/I balance and modulate downstream information flow in the hippocampus
190 that favors the encoding of new social information in its ventral subregions.

191 Our work provides mechanistic evidence for a hypothalamic content-specific novelty signal that
192 can contribute to shaping the engagement of distinct hippocampal subregions during encoding of
193 different types of memory. SuM modulation is probably not the sole source of such distinct
194 specificity; however, our findings demonstrate that within this small hypothalamic nucleus,
195 distinct novelty features can be detected, segregated and transmitted. How differences in input
196 circuitry permit novelty segregation in the SuM and how the signaling of segregated novelty
197 modifies hippocampal activity on the physiological level during behavior await further
198 investigation.

199

1 Ranganath, C. & Rainer, G. Neural mechanisms for detecting and remembering novel events. *Nat Rev Neurosci* **4**, 193-202, doi:10.1038/nrn1052 (2003).

2 van Kesteren, M. T., Ruiter, D. J., Fernandez, G. & Henson, R. N. How schema and novelty augment memory formation. *Trends Neurosci* **35**, 211-219, doi:10.1016/j.tins.2012.02.001 (2012).

3 Kafkas, A. & Montaldi, D. How do memory systems detect and respond to novelty? *Neurosci Lett* **680**, 60-68, doi:10.1016/j.neulet.2018.01.053 (2018).

4 Lisman, J. E. & Grace, A. A. The hippocampal-VTA loop: controlling the entry of information into long-term memory. *Neuron* **46**, 703-713, doi:10.1016/j.neuron.2005.05.002 (2005).

5 McNamara, C. G., Tejero-Cantero, A., Trouche, S., Campo-Urriza, N. & Dupret, D. Dopaminergic neurons promote hippocampal reactivation and spatial memory persistence. *Nat Neurosci* **17**, 1658-1660, doi:10.1038/nn.3843 (2014).

6 Duszkiewicz, A. J., McNamara, C. G., Takeuchi, T. & Genzel, L. Novelty and Dopaminergic Modulation of Memory Persistence: A Tale of Two Systems. *Trends Neurosci*, doi:10.1016/j.tins.2018.10.002 (2018).

7 Takeuchi, T. *et al.* Locus coeruleus and dopaminergic consolidation of everyday memory. *Nature* **537**, 357-362, doi:10.1038/nature19325 (2016).

8 Pan, W. X. & McNaughton, N. The supramammillary area: its organization, functions and relationship to the hippocampus. *Prog Neurobiol* **74**, 127-166, doi:10.1016/j.pneurobio.2004.09.003 (2004).

9 Saper, C. B. & Lowell, B. B. The hypothalamus. *Curr Biol* **24**, R1111-1116, doi:10.1016/j.cub.2014.10.023 (2014).

10 Wirtshafter, D., Stratford, T. R. & Shim, I. Placement in a novel environment induces fos-like immunoreactivity in supramammillary cells projecting to the hippocampus and midbrain. *Brain Res* **789**, 331-334, doi:10.1016/s0006-8993(97)01555-2 (1998).

11 Ito, M., Shirao, T., Doya, K. & Sekino, Y. Three-dimensional distribution of Fos-positive neurons in the supramammillary nucleus of the rat exposed to novel environment. *Neurosci Res* **64**, 397-402, doi:10.1016/j.neures.2009.04.013 (2009).

12 Kobayashi, Y. *et al.* Genetic dissection of medial habenula-interpeduncular nucleus pathway function in mice. *Front Behav Neurosci* **7**, 17, doi:10.3389/fnbeh.2013.00017 (2013).

13 Allen Institute for Brain Science. Allen Mouse Brain Atlas. Available from: mouse.brain-map.org/gene/show/12767 (2006).

14 Hama, H. *et al.* ScaleS: an optical clearing palette for biological imaging. *Nat Neurosci* **18**, 1518-1529, doi:10.1038/nn.4107 (2015).

15 Soussi, R., Zhang, N., Tahtakran, S., Houser, C. R. & Esclapez, M. Heterogeneity of the supramammillary-hippocampal pathways: evidence for a unique GABAergic neurotransmitter phenotype and regional differences. *Eur J Neurosci* **32**, 771-785, doi:10.1111/j.1460-9568.2010.07329.x (2010).

16 Reijmers, L. G., Perkins, B. L., Matsuo, N. & Mayford, M. Localization of a stable neural correlate of associative memory. *Science* **317**, 1230-1233, doi:10.1126/science.1143839 (2007).

17 Hunsaker, M. R., Rosenberg, J. S. & Kesner, R. P. The role of the dentate gyrus, CA3a,b, and CA3c for detecting spatial and environmental novelty. *Hippocampus* **18**, 1064-1073, doi:10.1002/hipo.20464 (2008).

18 Pedersen, N. P. *et al.* Supramammillary glutamate neurons are a key node of the arousal system. *Nat Commun* **8**, 1405, doi:10.1038/s41467-017-01004-6 (2017).

19 Hashimotodani, Y., Karube, F., Yanagawa, Y., Fujiyama, F. & Kano, M. Supramammillary Nucleus Afferents to the Dentate Gyrus Co-release Glutamate and GABA and Potentiate Granule Cell Output. *Cell Rep* **25**, 2704-2715 e2704, doi:10.1016/j.celrep.2018.11.016 (2018).

20 Tritsch, N. X., Granger, A. J. & Sabatini, B. L. Mechanisms and functions of GABA co-release. *Nat Rev Neurosci* **17**, 139-145, doi:10.1038/nrn.2015.21 (2016).

21 Boehringer, R. *et al.* Chronic Loss of CA2 Transmission Leads to Hippocampal Hyperexcitability. *Neuron* **94**, 642-655 e649, doi:10.1016/j.neuron.2017.04.014 (2017).
22 Resendez, S. L. *et al.* Social Stimuli Induce Activation of Oxytocin Neurons Within the Paraventricular Nucleus of the Hypothalamus to Promote Social Behavior in Male Mice. *J Neurosci* **40**, 2282-2295, doi:10.1523/JNEUROSCI.1515-18.2020 (2020).
23 Wu, Z., Autry, A. E., Bergan, J. F., Watabe-Uchida, M. & Dulac, C. G. Galanin neurons in the medial preoptic area govern parental behaviour. *Nature* **509**, 325-330, doi:10.1038/nature13307 (2014).
24 Strange, B. A., Witter, M. P., Lein, E. S. & Moser, E. I. Functional organization of the hippocampal longitudinal axis. *Nat Rev Neurosci* **15**, 655-669, doi:10.1038/nrn3785 (2014).
25 Leutgeb, J. K., Leutgeb, S., Moser, M. B. & Moser, E. I. Pattern separation in the dentate gyrus and CA3 of the hippocampus. *Science* **315**, 961-966, doi:10.1126/science.1135801 (2007).
26 Senzai, Y. & Buzsaki, G. Physiological Properties and Behavioral Correlates of Hippocampal Granule Cells and Mossy Cells. *Neuron* **93**, 691-704 e695, doi:10.1016/j.neuron.2016.12.011 (2017).
27 Danielson, N. B. *et al.* Distinct Contribution of Adult-Born Hippocampal Granule Cells to Context Encoding. *Neuron* **90**, 101-112, doi:10.1016/j.neuron.2016.02.019 (2016).
28 McHugh, T. J. *et al.* Dentate gyrus NMDA receptors mediate rapid pattern separation in the hippocampal network. *Science* **317**, 94-99, doi:10.1126/science.1140263 (2007).
29 Wintzer, M. E., Boehringer, R., Polygalov, D. & McHugh, T. J. The hippocampal CA2 ensemble is sensitive to contextual change. *J Neurosci* **34**, 3056-3066, doi:10.1523/JNEUROSCI.2563-13.2014 (2014).
30 Chiang, M. C., Huang, A. J. Y., Wintzer, M. E., Ohshima, T. & McHugh, T. J. A role for CA3 in social recognition memory. *Behav Brain Res* **354**, 22-30, doi:10.1016/j.bbr.2018.01.019 (2018).
31 Hitti, F. L. & Siegelbaum, S. A. The hippocampal CA2 region is essential for social memory. *Nature* **508**, 88-92, doi:10.1038/nature13028 (2014).
32 Stevenson, E. L. & Caldwell, H. K. Lesions to the CA2 region of the hippocampus impair social memory in mice. *Eur J Neurosci* **40**, 3294-3301, doi:10.1111/ejn.12689 (2014).
33 Piskorowski, R. A. *et al.* Age-Dependent Specific Changes in Area CA2 of the Hippocampus and Social Memory Deficit in a Mouse Model of the 22q11.2 Deletion Syndrome. *Neuron* **89**, 163-176, doi:10.1016/j.neuron.2015.11.036 (2016).
34 Alexander, G. M. *et al.* Social and novel contexts modify hippocampal CA2 representations of space. *Nat Commun* **7**, 10300, doi:10.1038/ncomms10300 (2016).
35 Smith, A. S., Williams Avram, S. K., Cymerblit-Sabba, A., Song, J. & Young, W. S. Targeted activation of the hippocampal CA2 area strongly enhances social memory. *Mol Psychiatry* **21**, 1137-1144, doi:10.1038/mp.2015.189 (2016).
36 Meira, T. *et al.* A hippocampal circuit linking dorsal CA2 to ventral CA1 critical for social memory dynamics. *Nat Commun* **9**, 4163, doi:10.1038/s41467-018-06501-w (2018).

Acknowledgments

We would like to thank Charles Yokoyama and Yu Mu for comments on the manuscript. We thank Jiamin Shi and Xiyu Wang for experimental support, Hiroshi Kurokawa for help with preparing image data, Michiko Fujisawa and Yuko Goto for daily assistance, the Advanced Manufacturing Support Team, RIKEN Center for Advanced Photonics for their assistance in microdrive production and all the members of the Lab for Circuit and Behavioral Physiology for advice. We thank Joshua Johansen for advice and reagents for rabies tracing and Shigeyoshi Itohara for supplying the Rosa-NLSLacZ Cre reporter mouse. This work was supported by JSPS (Japan Society for the Promotion of Science) Postdoctoral Fellowship (16F16386) (S.C.), RIKEN Special Postdoctoral Researchers Program (S.C.), Human Frontier Science Program Postdoctoral Fellowship (LT000579/2018) (S.C.), Grant-in-Aid for Young Scientists from MEXT (the Ministry of Education, Culture, Sports, Science and Technology of Japan) (16K18373, 18K14857) (S.C.), RIKEN Incentive Research Project Grant for Individual Germinating Research (S.C.), Narishige Neuroscience Research Foundation Grant (S.C.), Nakatani Foundation Grant Program (S.C.), Grant-in-Aid for Scientific Research from MEXT (19H05646; T.J.M) (16H04663; H.H.), Grant-in-Aid for Challenging Exploratory Research from MEXT (15K14357; T.J.M) (17K19451; H.H.), Grant-in-Aid for Scientific Research on Innovative Areas from MEXT (17H05591, 17H05986, 19H05233; T.J.M) (15H05948; A.M), (15H01430, 18H04743; H.H.), Brain/MINDS from AMED (JP18dm0207064; H.H.), the NeurImag facility at IPNP, the Foundation Recherche Médicale (FRM:FTD20170437387; V.R.), a NARSAD independent investigator grant from the Brain and Behavior Research Foundation (R.A.P.), Ville de Paris Programme Emergences (R.A.P.), Agence nationale de la recherche (ANR-13-JSV4-0002-01, ANR-18-CE37-0020-01;R.A.P) and RIKEN BSI and CBS (T.J.M).

Author contributions

S.C. conceived the study and mainly conducted experiments and analyzed data under guidance and supervision of T.J.M. S.C., L.H., Y.T., A.J.H. and T.J.M performed tracing and histology. S.C., L.H., M.E.W. and A.Z.W. performed behavioral experiments. S.C. performed in vivo electrophysiology and analyzed data; R.B. and L.H. contributed to data collection; D. P. and S.J.M contributed to data analysis. T.J.M. and A.J.H. generated the mouse lines. A.J.H. produced all AAVs. V.R., L.T., V.C. and R.A.P. performed in vitro electrophysiology,

immunohistochemistry and analysis. K.N., H. Hama and A.M. performed Sca*l*e; H. Hioki provided AAV vectors for Sca*l*e. All figures were prepared by S.C. with inputs from all authors. S.C. and T.J.M. wrote the manuscript. All authors discussed the manuscript.

Data availability

Data supporting the findings of this study are available from the corresponding authors upon reasonable request.

Code availability

Custom code used in this study is available from the corresponding authors upon reasonable request.

Methods

Animals. All mouse lines were maintained on a C57BL/6J background, bred in-house and raised in a temperature- and humidity-controlled room with a 12 h light/dark cycle (lights on from 08:00 A.M. to 8:00 P.M.). All experimental protocols were approved by the RIKEN Institutional Animal Care and Use Committee, animal protocol approval W2019-2-045 (2) and recombinant DNA approval Sho2018-013(9), Sho2019-054(1), Sho2018-014(1).

Generation of the SuM-Cre (Csf2rb2-Cre) mouse line. The bacterial artificial chromosome (BAC) RP23-233L7 (BACPAC Resources Center) containing the colony stimulating factor 2 receptor, beta2 (*csf2rb2*) was modified using the Quick & Easy BAC Modification Kit (Gene Bridges GmbH) to insert a Cre-FRT-Amp-FRT cassette at the start site of *csf2rb2* translation. The ampicillin (Amp) marker was deleted utilizing Flp-706 recombination and the Cre-modified BAC's were confirmed by PCR analysis. The confirmed Cre-modified RP23-233L7 BAC was subsequently purified using the QIAGEN Large Construct Kit (QIAGEN). To prepare the modified BAC for microinjection, 50 µg of Cre-modified RP23-233L7 BAC was linearized using AscI (New England Biolabs (NEB)) and then buffer exchanged using the Sepharose CL-4B matrix (Pharmacia/Pfizer) into an injection buffer composed of 10 mM Tris-HCl, pH 7.4, 0.1 mM EDTA, and 100 mM NaCl. The purified BAC was injected into C57BL/6 fertilized pronuclei and fertilized blastocysts were implanted into pseudopregnant females. From the microinjections, four *Csf2rb2-Cre* B6 founders (lines 252, 267, 271, 272) were generated. The 252 *Csf2rb2-Cre* line was determined to express Cre selectively in the supramammillary area of the hypothalamus using immunohistochemistry with the anti-Cre recombinase antibody (Millipore, MAB 3120). The 252 line was maintained in a pure C57BL/6 background for all the experiments herein described and male mice between the ages of 2 and 5 months were used for all experiments.

Generation of the SuM-Cre/ Rosa-NLSLacZ mouse line. The *252 Csf2rb2-Cre* line was bred with the *Rosa-NLSLacZ*[12] line. The double transgenic *252 Csf2rb2-Cre* x *Rosa-NLSLacZ* mouse line was confirmed with PCR genotyping for both the Cre and *β*-Gal genes and designated as R252. The two lines used to generate the double transgenic line were maintained in a pure C57BL/6 background for all the experiments herein described.

Generation of the SuM-Cre/c-Fos-tTA mouse line. The 252 *Csf2rb2-Cre* line was bred with the *Tg(Fos-tTA, Fos-EGFP*)1Mmay* line (JAX 018306)[16]. The double transgenic *252 Csf2rb2-Cre* x *Tg(Fos-tTA, Fos-EGFP*)1Mmay* mouse line was confirmed with PCR genotyping for both the Cre and EGFP genes and designated as I252. The two lines used to generate the double transgenic line were maintained in a pure C57BL/6 background for all the experiments herein described and male I252 mice between the ages of 2 and 5 months were used for all experiments.

Adeno-associated viruses (AAV) vector constructions. The pAAV.EF1a.DIO.hChR2(H134R).EYFP and pAAV.EF1a.DIO.eNpHR3.0.EYFP recombinant AAV vectors were obtained from the Deisseroth Laboratory (Stanford University). The pAAV.SynTetOff.DIO.EGFP and pAAV.SynTetOff.DIO.mCherry recombinant AAV vectors were obtained from the Hioki Laboratory (Kyoto University).

The recombinant AAV vectors pAAV.EF1a.DIO.EYFP and pAAV.EF1a.DIO.mCherry were generated at our laboratory. For the construction of pAAV.EF1a.DIO.EYFP, the EYFP fragment was generated using the high fidelity Phusion DNA Polymerase (NEB). At the 5' end of the DNA fragment, the NheI restriction enzyme site is followed by the Kozak sequence and 5' ORF of the EYFP from the pAAV.DIO.hChR2(H134R).EYFP plasmid (Stanford University). The 3' end of the EYFP ORF contains the AscI restriction enzyme site. The PCR-generated cassette was digested with NheI (NEB) and AscI (NEB). The vector backbone for this construct was the pAAV.EF1a.hChR2(H134R).EYFP plasmid digested with NheI and AscI and treated with calf intestine phosphate (NEB). The approximately 5.7 kB DNA fragment containing the vector backbone was ligated to the digested EYFP ORF DNA fragment with T4 DNA ligase buffer (NEB) and transformed into One Shot Stbl3 Chemically Competent Cells (Invitrogen) and colonies were screened by restriction digest analysis. The putative positive colonies were submitted for DNA sequencing and one clone with the correct DNA sequence was designated as pAAV.EF1a.DIO.EYFP.

For the construction of pAAV.EF1a.DIO.mCherry, the mCherry fragment was generated using the high fidelity Phusion DNA Polymerase (NEB). At the 5' end of the DNA fragment, the NheI restriction enzyme site is followed by the Kozak sequence and 5' ORF of the mCherry from the pAAV.DIO.hChR2(H134R).mCherry plasmid (Stanford University). The 3' end of the mCherry ORF contains the AscI restriction enzyme site. The PCR-generated cassette was digested with

NheI (NEB) and AscI (NEB). The vector backbone for this construct was the pAAV.EF1a.hChR2(H134R).EYFP plasmid digested with NheI and AscI and treated with calf intestine phosphate (NEB). The approximately 5.7 kB DNA fragment containing the vector backbone was ligated to the digested EYFP ORF DNA fragment with T4 DNA ligase buffer (NEB) and transformed into One Shot Stbl3 Chemically Competent Cells (Invitrogen) and colonies were screened by restriction digest analysis. The putative positive colonies were submitted for DNA sequencing and one clone with the correct DNA sequence was designated as pAAV.EF1a.DIO.EYFP.

Subsequently, the recombinant AAV vector pAAV.TRE.DIO.EYFP was generated at our laboratory. For the construction of pAAV.TRE.DIO.EYFP, the TRE promoter fragment was generated by digestion of the pAAV.TRE.EYFP plasmid (previously described Chen, Weitemier, et al.) with MluI (NEB) and XbaI (NEB). The vector backbone for this construct was the pAAV.EF1a.DIO.EYFP plasmid digested with MluI and XbaI and treated with calf intestine phosphate (NEB). The approximately 4.8 kB DNA fragment containing the vector backbone was ligated to the digested TRE promoter DNA fragment with T4 DNA ligase buffer (NEB) and transformed into One Shot Stbl3 Chemically Competent Cells (Invitrogen) and colonies were screened by restriction digest analysis. The putative positive colonies were submitted for DNA sequencing and one clone with the correct DNA sequence was designated as pAAV.TRE.DIO.EYFP.

For the rabies virus experiments, the recombinant AAV vector pAAV.EF1a.DIO.TVA950 was generated at our laboratory. For the construction of pAAV.EF1a.DIO.TVA950, the EF1a promoter fragment was generated by digestion of the pAAV.EF1a.DIO.mCherry with MluI (NEB) and XbaI (NEB). The vector backbone for this construct was the pAAV.UbiquitinC.DIO.TVA950 (Johansen Laboratory, RIKEN Center for Brain Science) plasmid digested with MluI and XbaI and treated with calf intestine phosphate (NEB). The approximately 4.8 kB DNA fragment containing the vector backbone was ligated to the digested EF1a promoter DNA fragment with T4 DNA ligase buffer (NEB) and transformed into One Shot Stbl3 Chemically Competent Cells (Invitrogen) and colonies were screened by restriction digest analysis. The putative positive colonies were submitted for DNA sequencing and one clone with the correct DNA sequence was designated as pAAV.EF1a.DIO.TVA950.

Finally, the recombinant AAV vector pAAV.EF1a.DIO.H2B.GFP.2A.oG was generated at our laboratory. For the construction of pAAV.EF1a.DIO.TVA950, the EF1a promoter fragment was generated by digestion of the pAAV.EF1a.DIO.mCherry with MluI (NEB) and XbaI (NEB). The vector backbone for this construct was the pAAV.UbiquitinC.DIO.H2B.GFP.2A.oG (Johansen Laboratory, RIKEN Center for Brain Science) plasmid digested with MluI and XbaI and treated with calf intestine phosphate (NEB). The approximately 7.2 kB DNA fragment containing the vector backbone was ligated to the digested EF1a promoter DNA fragment with T4 DNA ligase buffer (NEB) and transformed into One Shot Stbl3 Chemically Competent Cells (Invitrogen) and colonies were screened by restriction digest analysis. The putative positive colonies were submitted for DNA sequencing and one clone with the correct DNA sequence was designated as pAAV.EF1a.DIO.H2B.GFP.2A.oG.

AAV and Rabies Virus Preparation. For adeno-associated virus production, we used the AAV Helper Free System (Agilent Technologies). The adeno-associated virus vectors, pAAV.DIO.EYFP, pAAV.TRE.DIO.EYFP, pAAV.DIO.hChR2(H134R).EYFP, and pAAV.DIO.eNpHR3.0.EYFP were individually co-transfected with pAAV-DJ/8 (Cell Biolabs), which supplies AAV2 replication proteins and AAV-DJ/8 capsid proteins, and pHelper (Agilent Technologies) which supplies the necessary adenovirus gene products required for the AAV production into the 293FT cell line (Invitrogen) utilizing the 293fectin transfection reagent (Invitrogen). The adeno-associated virus vectors, pAAV.DIO.EYFP, AAV.DIO.mCherry, pAAV.SynTetOff.DIO.EGFP, pAAV.SynTetOff.DIO.mCherry, pAAV.EF1a.DIO.TVA950 and pAAV.EF1a.DIO.H2B.GFP.2A.oG were individually co-transfected with pretroAAV (Addgene), which supplies AAV2 replication proteins and retrograde AAV capsid proteins, and pHelper (Agilent Technologies) which supplies the necessary adenovirus gene products required for the AAV production into the 293FT cell line (Invitrogen) utilizing the 293fectin transfection reagent (Invitrogen). For the AAV.DJ/8 serotype AAV's, the supernatant was collected after 72 hours and centrifuged at 3,000 rpm for 30 minutes and then filtered through a 0.45μM filtration unit (Millipore). For the retrograde serotype AAV's, the supernatant and cells were collected after 72 hours and subjected to 3 cycles of freeze-thaw at −80°C and 37°C. The whole cell lysate and supernatant were then centrifuged at 3,000 rpm for 30 minutes and then filtered through a 0.45μM filtration unit (Millipore). Subsequent purification of the DJ/8 serotype AAV and retrogarde serotype AAV was carried out by ultracentrifugation (87,000 g, 4°C, 2 h) with a 20%

sucrose cushion. After ultracentrifugation, the supernatant was removed and the pellet was resuspended in phosphate-buffered saline (PBS), aliquoted and stored at −80°C for long term storage. The AAV stocks were titered using a custom ordered AAV stock purchased from Virovek (Hayward, CA) as the reference standard. AAV titer quantification was performed using qPCR with the StepOne Plus Real Time PCR System (Applied Biosystems), FastStart Universal SYBR Green Master (Roche, Basel), and QPCR primers for an approximately 100 bp fragment of the woodchuck hepatitis virus posttranscriptional response element (WPRE) found in all our adeno-associated virus vectors. The titers for the five AAV stocks ranged between 10^{12} to 10^{13} viral genome (vg)/mL for the DJ/8 serotype AAV's and between 10^{11} to 10^{12} viral genome (vg)/mL for the retrograde serotype AAV's. For the pseudotyped SAD rabies virus, the EnvA.RV.mCherry was generously provided by the Johansen Lab (RIKEN Center for Brain Science). The titer of the EnvA.RV.mCherry rabies virus was approximately 10^{9} infectious units (I.U.)/mL.

Stereotaxic injection and optic fiber implants. All surgeries were performed in a stereotaxic frame (Narishige). Mice were anaesthetized using 500 mg/kg Avertin. AAV's were injected using a 10 µL Hamilton microsyringe (701LT, Hamilton) with a beveled 33 gauge needle (NF33BL, World Precision Instruments (WPI)). A microsyringe pump (UMP3, WPI) and its controller (Micro4, WPI) were used to control the speed of the injection. The needle was slowly lowered to the target site and remained in place for 5 min before the beginning of the injection. AAVs were typically injected at a speed of 100 nL/min. The needle was removed 10 min after infusion was complete. Injections were targeted to the SuM (−2.7 mm AP, +0.4 mm ML, −5.0 mm DV), bilaterally to the DG (−1.9 mm AP, +/−1.2 mm ML, −2.1 mm DV) and CA2 (−1.9 mm AP, +/−2.2 mm ML, −1.8 mm DV).

The same procedure was used for CTB injections. For the dual fluorescence tracing visualization, injections of Alexa Fluor 488 CTB (1 mg/mL, 100 nL, Thermo Fisher) were targeted bilaterally to the DG while the Alexa Fluor 594 CTB (1 mg/mL, 100 nL Thermo Fisher) injections were targeted bilaterally to CA2.

For retrograde tracing of upstream inputs to the DG and CA2 projecting SuM neurons, retrograde AAV.EF1a.DIO.TVA950 and retrograde AAV.EF1a.DIO.H2B.GFP.2A.oG, injections were targeted bilaterally to the DG or CA2. Twenty-one days post-AAV injections,

the EnvA.RV.mCherry SAD rabies virus was targeted to the SuM and performed as described for the stereotaxic AAV injections above.

Optic fibers (200 μm core diameter) were bilaterally lowered above the target site (DG: −1.9 mm AP, +/− 1.2 mm ML, −1.7 mm DV; CA2: −1.9 mm AP, +/− 2.2 mm ML, −1.6 mm DV). The implant was secured to the skull with two jewelry screws and black opaque dental cement, which also prevented light leakage from the skull.

Immunohistochemistry and histology. Mice were transcardially perfused with 4% paraformaldehyde (PFA) in 0.1 M PBS (Nacalai Tesque). Brains were post-fixed in 4% PFA and 50 μm thick vibratome sections were prepared on a Vibratome (Leica).

Anti-*ß*-galactosidase immunohistochemistry. After 3 x 10 min PBS washes, the sections were blocked in TNB (Tris-NaCl blocking buffer) with 3% normal goat serum for 1.5 h, and incubated in primary antibody (goat anti-ß-galactosidase, 1:500, Abcam) at 4°C for 20 h. After 3 x 10 min washes in TNT (Tris-NaCl-Tween-20), the sections were incubated with secondary antibody (goat anti-chicken IgY, Alexa Fluor 488, 1:200, Abcam) for 2 h at room temperature followed by 3 x 10 min washes in TNT. Fluorescence images were acquired on the Keyence BZ-X810 All-in-One fluorescence microscope with either a 4x or 10x objective.

Anti-GFP immunohistochemistry. Anti-GFP immunohistochemistry was performed to label SuM cells infected by retrograde AAV.EF1a.DIO.H2B.GFP.2A.oG injected into DG or CA2. After 3 x 10 min PBS washes, the sections were blocked in TNB (Tris-NaCl blocking buffer) with 3% normal donkey serum for 1.5 h, and incubated in primary antibody (goat anti-GFP, 1:200, Abcam) at 4°C for 20 h. After 3 × 15 min washes in TNT (Tris-NaCl-Tween-20), the sections were incubated with secondary antibody (donkey anti-goat IgG, 1:200, Abcam) for 1 h at room temperature followed by 3 × 15 min washes in TNT. The sections were then incubated with a working solution for the TSA Plus Fluorescein Amplification Reagent (PerkinElmer) for 10 min at room temperature followed by 3 x 5 min washes in TNT. Fluorescence images were acquired on the Keyence BZ-X810 All-in-One fluorescence microscope with either a 4x or 10x objective.

Anti-PCP4 immunohistochemistry. After 3 x 10 min PBS rinses, the sections were blocked in PBST (PBS + 0.3% Triton X-100) with 3% normal donkey serum for 1.5 h, and incubated in

primary antibody (rabbit anti-PCP4, 1:1000, Santa Cruz Biotechnologies) at 4°C for 20 h. After 3 x 10 min washes in PBS, the sections were incubated with secondary antibody (donkey anti-rabbit, Alexa Fluor 594, 1:500, Life Technologies) for 2 h at room temperature followed by 3 x 10 min washes in PBS. Confocal fluorescence images were acquired on an Olympus IX81 confocal laser scanning microscope with a 10x or 20x objective.

Anti-c-Fos immunohistochemistry and histology. After 3 x 10 min PBS rinses, the sections were blocked in PBST (PBS + 0.3% Triton X-100) with 3% normal donkey serum for 1.5 h, and incubated in primary antibody (rabbit anti-c-Fos, 1:1000, Synaptic Systems) at 4°C for 20 h. After 3 x 10 min washes in PBS, the sections were incubated with secondary antibody (donkey anti-rabbit, Alexa Fluor 594, 1:500, Life Technologies) for 2 h at room temperature followed by 3 x 10 min washes in PBS.

Confocal fluorescence images were acquired on an Olympus IX81 confocal laser scanning microscope with a 20x objective. To calculate the c-Fos+ cell density in Fig. 1b, three 50 μm-thick sections at representative SuM coordinates (AP: -2.5, -2.8 and -3.0 mm, as shown in Fig. 2b) were prepared from each animal and imaged. The total number of c-Fos+ cells in the SuM across the three sections was counted and divided by the total area of the SuM region to derive the c-Fos+ cell density. Data from four animals was obtained for each condition (exposure to a familiar context, a novel context or a novel animal) and plotted. To analyze the overlap between fluorescent markers (anti-c-Fos and EYFP, mCherry and EYFP), a z-stack function was used to montage 5 optical stacks (1 μm each, step size 4 μm). Filtered fluorescent images were digitally combined to produce composite images and the number of cells with overlapping signals was counted in the region of interest (ROI) with ImageJ. The overlap ratio in Fig. 3d was calculated as (number of cells labeled in both green and red) / (total number of cells labeled in green). The overlap ratio in Fig. 3j was calculated as (number of cells labeled in both green and red) / (number of cells labeled in red). The overlap ratio in Extended Data Fig. 8f was calculated as (number of cells labeled in both green and red) / (number of cells labeled in green). For statistics, slices from at least 3 animals were obtained, imaged and analyzed. All imaging and analyses were performed blind to the experimental conditions.

RNAscope. Mice were transcardially perfused with 4% PFA in 0.1 M PBS (Nacalai Tesque). Brains were post-fixed in 4% PFA and 50 μm-thick vibratome sections were prepared on a

Vibratome (Leica). RNAscope hybridization was performed using the RNAscope Multiplex Fluorescent Reagent Kit v2 Assay (Advanced Cell Diagnostics). After 4 × 10 min TBS washes, free-floating slices were treated with pretreatment solutions of proprietary compositions (Advanced Cell Diagnostics). First, the slices were placed RNAscope Hydrogen Peroxide for 30 minutes at 25˚C, followed by 2 x 1 min 1x TBS washes, and 2 x 1 min 0.5x TBS washes, the slices were mounted on Superfrost Plus Slides (Fisher Scientific) were baked in a dry oven for 1 h at 60°C. The mounted slices were then placed in Target Retrieval Reagent for 15 min at 100–104°C, followed by washes in ddH_2O and then 100% ethanol. The slices were baked in a dry oven for 30 min at 60˚C. The slices were then placed in RNAscope Protease Plus for 30 min at 40°C followed by 2x washes in ddH_2O. The slices were incubated with the following trio of RNAscope probes, Mm-Slc17a6 (vGluT2), Mm-Slc32a1-C3 (vGAT), and EYFP-C2 (Advanced Cell Diagnostics) for 2 h at 40°C, followed by amplifying hybridization processes, AMP1, AMP2, and AMP3. The RNAscope probes were developed in the following order: Mm-Slc17a6 HRP-C1.Opal 570, Mm-Slc32a1-C3.Opal 690, and lastly EYFP-C2.Opal 520 (Ayoka Biosciences). The slices were counterstained with RNAscope 4',6-diamidino-2-phenylindole (DAPI) (Advanced Cell Diagnostics) for 1 min at 25°C followed by 1 – 2 drops of Prolong Gold Antifade Mountant (Thermo Fisher) before placing coverslip and sealing slides. Fluorescence images were acquired on the Keyence BZ-X810 All-in-One fluorescence microscope with either a 4x or 10x objective.

Sca*l*eS and AbSca*l*e. For selective plane illumination microscopy of whole brains, adult mice were deeply anesthetized with pentobarbital (Somnopentyl) and transcardially perfused with 4% PFA/PBS(-). The whole brain was extracted and subjected to post-fixation in 4% PFA/PBS(−) at 4°C for 24 hrs. Then, the brain samples were cleared by Sca*l*eS as described previously[23]. Observation was performed with a ZEISS Lightsheet Z.1 equipped with a 5x objective lens (Plan-Neofluor, NA = 0.16, RI = 1.45) and a 5x illumination lens (LSFM, NA = 0.1). The EYFP fluorescence was observed using a 488-nm diode laser and a 504–545 emission filter. A cleared sample was glued to the tip of a syringe (1 ml) and was positioned in front of the objective in the mounting medium (Sca*l*eS4). Images were acquired every 6.126 μm along the z-axis.

For c-Fos expression visualized by AbSca*l*e, a 0.8-mm-thick coronal brain slice was prepared from a SuM-Cre mouse infected with the Cre-dependent EYFP AAV. The EYFP fluorescent

images of 4%(w/v) PFA-fixed brain slices were acquired by a fluorescence stereo-microscope (Leica MZ16F) equipped with a 1× objective lens (Leica PLANAPO, NA = 0.141) and a color CCD camera (Zeiss AxioCam 506 color). The filters of ET-GFP (470 ± 20 nm) and ET-GFP (525 ± 25 nm) were used for excitation and emission, respectively. Then, AbSca*l*e was performed as described previously[14]. The brain slices were reacted with a Cy5-conjugated rabbit anti-cFos polyclonal antibody (F7799, Sigma) (1.67 μg protein/mL). Multiple adjacent regions in the slice were imaged with an upright laser scanning confocal microscopy system (Olympus FV1200) equipped with a motorized xy stage module in addition to a motorized focus module (z-drive), and a 10× dipping objective lens (Olympus XLPLN10XSVMP, NA = 0.6, WD = 6 mm, RI = 1.33–1.52). The EYFP fluorescence was observed using 473 nm laser. The Cy5 fluorescence was observed using 635 nm laser. The adjacent regions were overlapped by 10% for precise alignment. The z step size was 10 μm.

***In vivo* electrophysiology.** We recorded extracellularly from SuM neurons using custom-built screw-driven microdrives. The drives contain four to six independently adjustable nichrome tetrodes (14 mm), gold-plated to an impedance of 200 to 250 kΩ. The relative position of each tetrode exiting the cannulas on the bottom of the recording drive was mapped prior to surgery. The microdrive was implanted with the tetrodes placed approximately 4.5 mm ventral from the skull surface. Two days post-surgery, tetrodes were slowly lowered over several days to the SuM. As the tetrode were implanted at depth, we could ensure they entered the brain smoothly and perpendicularly, thus maintaining their relative positions even at their tip. During the adjustment period the animal was habituated every day in a same bucket for 15 min (Familiar Context) to ensure at least 10 days of habituation before the recordings started.

Recordings commenced once the SuM was reached based on the presence of theta oscillations and high amplitude spiking. At the start of each day the tetrodes were finely adjusted to maximize cell yield. Recordings started from 15-min exposure to the Familiar Context, followed by 5-min exposure to a Novel Context, a second 15-min exposure to the Familiar Context and a 5-min exposure to a Novel Animal.

Neural signals and time stamps for behavior were recorded using a DigiLynx recording system running Cheetah v 5.7.4 acquisition software (Neuralynx). Broadband signals from each wire filtered between 0.1 and 9,000 Hz were recorded continuously at 32 kHz. The location and head

direction of the animal were accurately tracked by the red and green diodes affixed above the animal's head.

After recordings were completed, mice underwent terminal anesthesia with Avertin and electrode positions were marked by electrolytic lesioning of brain tissue (30 mA current for 5 s through each tetrode). After transcardial perfusion with 4% PFA brains were removed and post-fixed for another 24 hr in 4% PFA. Coronal slices (50 μm thick) were prepared and inspected by standard light microscopy to confirm electrode placement. We cross-referenced the pattern of lesions across multiple sections with the tetrode positions mapped before the implantation of the recording drive to ensure precise positional assignment of each tetrode.

Circuit-specific optogenetic identification and recordings. The microdrive was fabricated in the same way as described above except for the inclusion of an optic fiber with precisely designed geometry to allow its placement above the CA2 or DG (DG: −1.9 mm AP, +/− 1.2 mm ML, −1.7 mm DV; CA2: −1.9 mm AP, +/− 2.2 mm ML, −1.6 mm DV). Same procedures for adjustment and recording were used, except for an additional optogenetic identification session in the beginning of the recording. In this session, trains of 10 light pulses (473nm, 10 mW/mm^2) were delivered to the CA2 or DG, each 20-ms long, at 10 Hz. Spike shape of the SuM neurons was simultaneously measured using a broadband signal (0.1–9,000 Hz) sampled at 32 kHz. Recording then continued without laser pulses as the mice explored a familiar context, a novel context and a novel animal. Recording sites were later verified histologically with electrolytic lesions as described above and the position of the optic fiber was also verified from the track.

Data analysis. Spikes were manually sorted with off-line software SpikeSort3D (Neuralynx). The mean firing rate of each neuron was calculated using the first 5-min of data recorded in each exposure condition. When two Familiar Context epochs were recorded in one recording, the firing rates of each neuron in both epochs were averaged to be the mean. Putative excitatory neurons (pEN) and inhibitory interneurons (pIN) were separated by the K-means clustering algorithm. In addition to a threshold of meaning firing rate (neurons with firing rate <10 Hz in all exposures were identified to be pEN), another two parameters, half-width of the spike and trough to peak duration, were taken into account. pENs have longer trough-to-peak durations and half-widths compared to pINs.

To determine whether a neuron's firing rate in the Novel Context or Novel Animal epoch was significantly different from that in the previous Familiar Context epoch, the spike train was circularly shifted by a random distance after removing the time gap between the two epochs by swapping a single spike at the joint. This shuffling process was repeated 1,000 times and the firing rate difference between the two shuffled epochs was calculated, to generate a *P*-value:

$$P = (n+1)/(r+1)$$

where r represents the total number of shuffles (1,000) and n is equal to the number of shuffles with a firing rate difference between the two epochs greater than or equal to the unshuffled value. Cells with a $P < 0.05$ were considered to have a significantly different firing rate from that in the Familiar Context epoch.

For calculating the change of the novelty response with time, firing rates of individual neurons in the three different exposures were binned in 30-s bins and normalized to the average Familiar Context firing rate of all identified neurons.

To identify individual DG- or CA2-projecting neurons by antidromic spiking, we used a combination of criteria including (a) early latency (< 20 ms from the onset of the light pulse), (b) high fidelity (in response to > 50% of light pulses), and (c) mean light-evoked waveform closely resembling the spontaneous waveform. Mean firing rates of the optogenetically identified cells in the Familiar Context, Novel Context and Novel Animal epochs were calculated and compared.

Behavioral tests and optogenetics. For the contextual memory test, a one-day contextual habituation protocol was used. Mice expressing ChR2, eNpHR or EYFP and with fibers delivering light to the DG or CA2 went through six contextual exposure session: Each was 5 min with 15 min intersession intervals. Mice were first placed in a novel high-walled square enclosure containing 2 objects and their movement was tracked by ANY-maze (Stoelting) as they explored for 5 min (Session A1). Following a 15 min intersession interval, mice were returned to the same context for three additional 5 min sessions (A2, A3 and A4) with 15 minutes intervals in between. Only during Session A4 light (circuit activation: 473 nm, 10 Hz, 30 ms pulse duration, 10 mW; circuit inhibition: 532 nm, constant, 5 mW) was bilaterally delivered to CA2 or DG for circuit manipulation. After a 15 minutes interval, mice were placed to a novel context for 5 min exploration with light bilaterally delivered to CA2 or DG (Session B1). Again,

after a 15-minute interval, mice were placed back to the context for a final 5 min session in the absence of light delivery (Session B2).

For social memory tests, a direct interaction test was used. Mice were first habituated in a context for ten days (15 min per day). On the day of social familiarity test, subject mice were exposed to a novel juvenile male mouse in the familiar context where the mice had been habituated and allowed to interact for 5 min without light stimulation and interaction time was scored. Following a 1 hour inter-trial interval the mice were re-exposed to the same juvenile demonstrator, with the appropriate wavelength light (circuit activation: 473 nm, 10 Hz, 30 ms pulse duration, 10 mW; circuit inhibition: 532 nm, constant, 5 mW) bilaterally delivered to CA2 or DG for circuit manipulation, and interaction time was scored. Habituation index was calculated as (time spent exploring the familiar mouse minus time spent exploring the stimulus mouse) / (time spent exploring the familiar mouse plus time spent exploring the stimulus mouse). In a social novelty test, the same procedure was used except that in the second trial mice were required to interact with a novel juvenile male mouse with light delivered. Habituation index was calculated as (time spent exploring the novel mouse minus time spent exploring the stimulus mouse) / (time spent exploring the novel mouse plus time spent exploring the stimulus mouse).

In vitro electrophysiology. For stereotaxic viral injection, animals were anaesthetized with ketamine (100 mg/kg) and xylazine (7 mg/kg). The adeno-associated virus AAV9.EF1a.DIO.hChR2(H134R).EYFP was used at $3x10^{8}$ vg/mL, AAV.retro.DIO.hChR2.EYFP was used at 1.5 x 10^{11} vg/mL. 500 nL of virus was injected into the brain of 4-week-old male csf2rb2-Cre (SuM-Cre) mice at 100 nL/min and left at the injection site for 10 min following infusion. The loci of the injection sites were as follows: for medial SuM, −2.8 mm anterior–posterior relative to bregma (A/P); 0 mm medial-lateral relative to midline (M/L); 4.75 mm dorsal-ventral relative to surface of the brain (D/V). For CA2, -1.7 A/P, 1.9 mm M/L, 1.6 mm D/V. For DG, -2.0 A/P, 1.2 mm M/L, 2.1 mm D/V.

Transverse hippocampal slices were prepared at least 3 weeks after viral injection and whole-cell patch-clamp recordings were performed from CA2 PNs and DG GCs. Animals were anaesthetized with ketamine (100 mg/kg) and xylazine (7 mg/kg), and perfused transcardially with a N-methyl-D-glucamin-based (NMDG) cutting solution containing the following (in mM): NMDG 93, KCl 2.5, NaH_2PO_4 1.25, $NaHCO_3$ 30, HEPES 20, glucose 25, thiourea 2, Na-

ascorbate 5, Na-pyruvate 3, $CaCl_2$ 0.5, $MgCl_2$ 10. Brains were then rapidly removed, hippocampi were dissected and placed upright into an agar mold and sliced with a vibratome (Leica VT1200S) in the same cutting solution into 400 µm thick transverse slices at 4°C. Slices were transferred to an immersed-type chamber and maintained in artificial cerebro-spinal fluid (ACSF) containing the following (in mM) : NaCl 125, KCl 2.5, NaH_2PO_4 1.25, $NaHCO_3$ 26, glucose 10, Na-pyruvate 2, $CaCl_2$ 2, $MgCl_2$ 1. Slices were incubated at 32°C for approximately 20 min then maintained at room temperature for at least 45 min prior to transfer to a recording chamber perfused with ACSF at 5 mL/min at 30°C. Whole-cell patch-clamp recordings were performed with a cesium-based intracellular solution containing the following (in mM): Cs-methyl sulfonate 130, KCl 5, EGTA-KOH 0.1, HEPES 10, NaCl 2, MgATP 5, Na_2GTP 0.4, Na_2-phosphocreatine 10 and biocytin (4 mg/mL). ChR2 expressed in SuM axonal fibers was excited by 488 nm light delivered by a LED attached to the epifluorescence port of the microscope. Light stimulation trains consisted of 2 to10 pulses that were 0.5 ms long, delivered at 10 Hz and repeated every 10–20 s for at least 20 sweeps. When blocking action potentials with TTX, light pulse duration was increased to 5 ms to allow direct depolarization of pre-synaptic SuM terminals (Extended Data Fig. 10). We used a light intensity of 25 mW/mm² which was experimentally determined to be the minimal intensity allowing TTX-sensitive maximal responses in all cell types. Data were obtained using a Multiclamp 700B amplifier, sampled at 10 kHz and digitized using a Digidata 1550B interface. Series resistance was < 20 MOhms and was continuously monitored in voltage-clamp mode. Liquid junction potential offset of approximately 10 mV was not corrected for. Pharmacological agents were added to ACSF at the following concentrations (in µM): 10 NBQX and 50 D-APV to block AMPA and NMDA receptors, 1 SR95531 and 2 CGP55845A to block GABAA and GABAB receptors, 100 4-Aminopyridine (4-AP) to block K_V1 potassium channels, 0.2 TTX to prevent action potential generation.

Midbrains containing the injection site were always examined post-hoc to ensure that infection was restricted to the SuM. Post-hoc reconstruction of neuronal morphology and SuM axonal projections were performed on slices and midbrain tissue following overnight incubation in 4% PFA in PBS. Midbrain sections were sagitally re-sliced to 100 µm thick sections. Because internal recording solutions contained Cs^+, we examined the cellular morphology and location of all cells post-hoc to ensure data were from CA2 PNs and DG GCs (Extended Data Fig. 10).

Slices were permeabilized with 0.2% Triton in PBS and blocked overnight with 3% goat serum in PBS with 0.2% Triton. Primary antibody incubation was carried out in 3% goat serum in PBS overnight at 4°C. Channelrhodopsin-2 was detected by chicken primary antibody to GFP (Abcam; 1:10,000 dilution) and Alexa Fluor 488-conjugated goat-anti chicken secondary (Life Technologies, 1:300 dilution). Incubations with secondary antibodies, Alexa Fluor 594-conjugated streptavidin (Life Technologies, 1:500 dilution) and Far-red Neurotrace (Life Technologies, 1:300 dilution), were carried out in block solution for 4 hours at room temperature. After a mounting with ProlongDiamond, images were collected with a Zeiss 710 or Leica SP5 laser-scanning confocal microscope.

Electrophysiological recordings were analyzed using IGORpro (Wavemetrics) and Clampfit (Molecular devices) software. For accurate measurements of the kinetics and latencies of post-synaptic responses, the following detection process was used. For each cell, average traces were used to create a template waveform that was then fitted to individual traces and measurements were performed on the fitted trace. When only amplitudes of responses were measured, standard average peak detection was used. Results are reported ± s.e.m. Statistical significance was assessed using unpaired- or paired-Student's T test, Mann-Whitney U test, Wilcoxon signed-rank test, or Kolmogorov-Smirnoff test where appropriate.

Statistics and reproducibility. All statistical analyses were performed with GraphPad Prism 7, Excel 2010 (Microsoft) or custom MATLAB codes. The sample sizes were chosen based on common practice in similar animal experiments[7,10,11,18,19,28,29,33-36]. Experimenters were blind to genotype, region targeted and optical protocol during injections and experiments, as well as during histological and behavioral analysis. For all experiments mice were randomly assigned as to which virus they received, the injection location and protocol used. Data were first tested for normality. When normality or equal variance between samples was achieved, parametric tests such as one-way ANOVA with Turkey's post hoc test or *t*-test were used. Where normality or equal variance of samples failed, nonparametric tests such as Wilcoxon signed rank test were performed. All values were presented as mean ± s.e.m. Representative example data in all figures was selected from multiple biological replicates; Fig. 1b: 1 of 4 mice, Fig. 1f: 6 example neurons of 119 units recorded from 17 mice, Fig. 2a, b: 1 of 10 mice, Fig. 2c: 1 of 3 mice, Fig. 2d, e: 1 of 6 mice, Fig. 3c, g, i: 1 of 3 mice, Fig. 3r: 4 example neurons of 29 units recorded from 19 mice,

747 Extended Data Fig. 1b: 1 of 4 mice, Extended Data Fig. 2b: 1 of 17 mice, Extended Data Fig. 3c,
748 d: 1 of 3 mice, Extended Data Fig. 4a: 1 of 10 mice, Extended Data Fig. 4b: 1 of 3 mice,
749 Extended Data Fig. 5a, b: 1 of 3 mice, Extended Data Fig. 6a: 1 of 6 mice, Extended Data Fig.
750 6b: 1 of 3 mice, Extended Data Fig. 6e, f: 1 of 2 mice, Extended Data Fig. 7a: 1 of 6 mice,
751 Extended Data Fig. 7b: 1 of 7 mice, Extended Data Fig. 8c, e: 1 of 3 mice, Extended Data Fig.
752 8h: 1 of 8 mice, Extended Data Fig. 8k: 1 of 11 mice, Extended Data Fig. 11c, e: 1 of 4 mice,
753 Extended Data Fig. 11d, f: 1 of 5 mice.

Figure 1 | **SuM responds to contextual and social novelty**. **a**, Following habituation mice are exposed to a novel context or a novel animal. **b**, c-Fos immunostaining in the SuM of mice after exposure to a familiar context, a novel context or a novel animal. Scale bar, 200 μm. **c**, Contextual and social novelty induce significant c-Fos expression in the SuM. One-way ANOVA with Tukey's post hoc test, $n = 4$ mice for all groups, $^{****}P < 0.0001$. Open circles represent values of individual mice. **d**, Behavioral recording protocol; sequential exposure to a familiar context, a novel context and a novel animal. **e**, Tetrodes targeting SuM. **f**, Example raster plots. Cells 1 and 2 were activated in a novel context, 3 and 4 were activated by a novel animal, and 5 and 6 responded to both contextual and social novelty. FR, firing rate. **g**, Mean FR of all pEN units ($n = 119$ cells from 17 mice) during novelty. One-way repeated measures ANOVA with Tukey's post hoc test, $^{*}P = 0.0240$, $^{****}P < 0.0001$. **h**, **i**, Scatter plots of the FRs of all pEN units during novel contextual (**h**) and novel social (**i**) exposures, plotted against FRs during familiar contextual exposure. Colored dots indicate neurons with significant increase in FR. Pie chart summarizes fraction of population. **j**, Venn diagram of overlap between subpopulations with significantly increased activity during novel contextual and novel social exposures. **k**, SuM neurons with a significant FR increase after exposure to a novel context (blue, $n = 26$ units) or animal (red, $n = 25$ units) displayed habituation. Black curve represents FR change of the union of the above two subsets of neurons ($n = 39$ units) in a familiar context. All error bars and shaded areas show mean ± s.e.m.

Figure 2 | SuM-Cre mice reveal robust SuM-hippocampal projections. **a**, Left: SuM injection of Cre-dependent AAV in SuM-Cre mice resulted in SuM-restricted eYFP (green) expression and strong terminal labeling in the DG and CA2 of the hippocampus. Right: Extent of axonal terminals (eYFP, green) of SuM neurons in hippocampus along the rostrocaudal axis, referenced to adapted atlas images. Scale bars, 1 mm. **b**, Cre-dependent eYFP expression in the SuM of SuM-Cre mice. Numbers indicate posterior distances from bregma. Scale bars, 200 μm. **c**, Left: Coronal hippocampal section showing axonal terminals of SuM neurons (eYFP, green) and hippocampal neurons immunostained with anti-PCP4 (red). Scale bar, 500 μm. Right: Magnified images from boxes on the left highlighting SuM axons targeting granule cells in the DG and pyramidal neurons in CA2, both PCP4 positive (red). Scale bars, 50 μm. **d**, **e**, Bilateral

injection of retroAAV-DIO-mCherry to hippocampal DG and retroAAV-DIO-EYFP to CA2 of the SuM-Cre mice selectively labels DG-projecting SuM neurons with mCherry and CA2-projecting SuM neurons with eYFP. Axons targeting the hippocampus are shown in **d** (scale bar, 500 μm), and soma in the SuM are shown in **e** (scale bars, 200 μm). Numbers in **e** indicate posterior distances from bregma.

Figure 3 | DG- and CA2-projecting SuM neurons respond to contextual and social novelty, respectively. **a**, Experimental design to examine the overlapping SuM populations that respond to two novelty exposures. **b**, Double transgenic mice (SuM-Cre/c-Fos-tTA) were injected with AAV-TRE-DIO-EYFP. **c**, Images of overlapping populations in the SuM activated by two novelty exposures. On the right of each image is a magnified view of the area within the white box (200 × 200 μm). **d**, eYFP+/c-Fos+ overlap SuM cell counts for the conditions shown in **c**. One-way ANOVA with Tukey's post hoc test, $n = 3$ mice for all groups, $^{****}P < 0.0001$. **e**, Protocol to examine the projection specificity of SuM populations that respond to novel contextual or social exposure. **f**, **h**, Strategy to simultaneously label DG- (**f**) or CA2- (**h**) projecting SuM cells using retroAAV-DIO-mCherry and novelty-responsive cells using AAV-TRE-DIO-EYFP with the SuM-Cre/c-Fos-tTA mice. **g**, **i**, Images of overlapping populations in the SuM that were activated by contextual or social novelty and projected to the DG or CA2. On the right of each image is a magnified view of the area within the white box (200 × 200 μm). **j**, eYFP+/mCherry+ overlap SuM cell counts for the conditions shown in **g** and **i**. One-way ANOVA with Tukey's post hoc test, $n = 3$ mice for all groups, $^{***}P = 0.0004$, $^{****}P < 0.0001$. **k**, Protocol for a recording session to optogenetically identify DG- or CA2-projecting SuM neurons. **l**, **o**, Viral injection, optic fiber and tetrodes implantation. **m**, **p**, Peristimulus time histograms of representative single units photoidentified as SuM-DG (**m**) and SuM-CA2 (**p**) projectors. **n**, **q**, Waveforms of spontaneous (grey) and light-evoked antidromic (blue) spikes of the single units in **n** and **q**. **r**, Raster plots of sample neurons. Cells 1 and 2 projecting to DG were more active in a novel context, and Cells 3 and 4 projecting to CA2 preferentially responded to a novel animal. FR, firing rate. **s**, **t**, Calculated FR changes of DG-projecting (**s**, $n = 12$ putative excitatory neurons from 8 mice, $^{**}P = 0.0024$) and CA2-projecting (**t**, $n = 17$ putative excitatory neurons from 11 mice, $^{***}P = 0.0003$) SuM neurons in response to

contextual and social novelty. FR change = (FR in Contextual or Social minus FR in Familiar) / (FR in Contextual or Social plus FR in Familiar). Two-tailed Wilcoxon matched-pairs signed rank test. All error bars show mean ± s.e.m. Open circles are values from individual mice. Scale bars, 200 μm.

Figure 4 | SuM-hippocampal circuits selectively modulate contextual and social memory. a, Protocol used for contextual memory tests. **b–e**, Distance traveled during each contextual exposure normalized to Session A1 under optogenetic manipulations of SuM-hippocampal circuits. Light was delivered in Sessions A4 and B1 to the DG or CA2. Two-way ANOVA with Bonferroni post hoc test, $n = 11$ mice (DG/ChR2) versus $n = 11$ (DG/eYFP) in **b** ($^{*}P = 0.0119$, $F(20, 100) = 2.961$), $n = 11$ (DG/eNpHR) versus $n = 9$ (DG/eYFP) in **c** ($^{****}P < 0.0001$, $F(18, 90) = 3.490$), $n = 11$ (CA2/ChR2) versus $n = 9$ (CA2/eYFP) in **d**, $n = 10$ (CA2/eNpHR) versus $n = 12$ (CA2/eYFP) in **e**. **f**, Protocol used for social familiarity tests. **g**, **h**, Habituation index with a familiar animal under various optogenetic manipulations of SuM-hippocampal circuits. Two-tailed unpaired *t*-tests, $n = 13$ mice (DG/ChR2) versus $n = 9$ (DG/eYFP), $n = 10$ (DG/eNpHR) versus $n = 11$ (DG/eYFP) in **g**, $n = 17$ (CA2/ChR2) versus $n = 19$ (CA2/eYFP), $n = 10$ (CA2/eNpHR) versus $n = 13$ (CA2/eYFP) in **h**, $^{***}P = 0.0008$, $t(34) = 3.665$. **i**, Protocol used for social novelty tests. **j**, **k**, Habituation index with a novel animal under various optogenetic manipulations of SuM-hippocampal circuits. Two-tailed unpaired *t*-tests, $n = 13$ mice (DG/ChR2) versus $n = 9$ (DG/eYFP), $n = 10$ (DG/eNpHR) versus $n = 11$ (DG/eYFP) in **j**, $n = 13$ (CA2/ChR2) versus $n = 10$ (CA2/eYFP), $n = 16$ (CA2/eNpHR) versus $n = 12$ (CA2/eYFP) in **k**. n.s., nonsignificant. Error bars show mean ± s.e.m. Boxes denote median (centre line), 25th and 75th percentiles (box edges), and full range of values (whiskers).

Extended Data Figure 1 | Identification of hypothalamic regions activated by contextual and social novelty. **a**, Counts of c-Fos+ cells in hypothalamic regions that show response to contextual and social novelty. $^{*}P = 0.0140$, $^{**}P = 0.0023$, $^{***}P = 0.0009$, $^{****}P < 0.0001$. n.s., nonsignificant. Two-way ANOVA with Tukey's post hoc test, $n = 4$ mice for all groups. Error bars indicate mean ± s.e.m. Open circles are values from individual mice. **b**, Example c-Fos immunostaining (red) in the hypothalamus of one mouse from a total of 4 replicates at various

distances from bregma along the rostrocaudal axis of mice 1.5 h after exposure to a familiar context, a novel context or a novel animal. AHN, anterior hypothalamic nucleus; DMH, dorsal medial hypothalamic nucleus; LHA, lateral hypothalamic area; LPO, lateral preoptic area; MM, medial mammillary nucleus; MPN, medial preoptic nucleus; MPO, medial preoptic area; PH, posterior hypothalamic nucleus; PVH, paraventricular hypothalamic nucleus; SuM, supramammillary nucleus; VMH, ventromedial hypothalamic nucleus. Scale bars, 500 μm.

Extended Data Figure 2 | Histology of recorded animals and firing rate analysis of interneurons. a, Tetrode recordings in the SuM. **b**, An example coronal section of the SuM from one of 17 mice used for recording with tetrode locations indicated by arrows. Scale bar, 400 μm. **c**, Reconstructed tetrode tip locations (71 in target and 14 off target) from 17 animals overlaid onto schematic mouse brain slices. Numbers indicate posterior distances from bregma. **d**, Behavioral protocol for a recording session, including sequential exposure to a familiar context, a novel context and a novel animal. **e**, Mean FR of all pIN (putative interneuron, $n = 22$ from 17 mice) units during different exposures. FR, firing rate. One-way repeated measures ANOVA. n.s., nonsignificant. **f**, **g**, Scatter plots of the FRs of all IN units during novel contextual (**f**) and novel social (**g**) exposures, plotted against FRs during familiar contextual exposure. Colored dots indicate interneurons that showed a significant increase in FR. Horizontal and vertical green bars indicate 10 Hz, the low threshold of FR to classify interneurons. Pie graphs show the percentage of pIN units that exhibited significant increase, significant decrease, or no change in FR during the respective novelty exposure. **h**, Venn diagram of overlap between subpopulations with significantly increased activity during novel contextual and novel social exposures.

Extended Data Figure 3 | Generation and characterization of the SuM-Cre mouse line. a, Recombination strategy for SuM-specific expression of Cre recombinase driven by the csf2rb2 promoter. Diagram shows the schematic of the csf2rb2 promoter.Cre.FRT.AmpR.FRT construct. **b**, Example anti-Cre immunostaining in the SuM of the SuM-Cre mouse (one of three replicates). Dotted white line indicates the anatomical boundary of the SuM. Scale bar, 500 μm. **c**, **d**, Coronal (**c**) and sagittal (**d**) sections (scale bars, 2 mm) prepared from an adult progeny (age 12 weeks) of SuM-Cre and Rosa-NLSLacZ crosses and immunostained with anti-*β*-galactosidase (*β*-gal, recombination marker). Representative images of from all brain regions where recombination is identified are shown from one mouse of four replicates of each. Dotted white lines indicate the boundaries of these brain regions. On the right of each image in **c** is a magnified view of the area within the white box (scale bars, 1 mm). BLA, basolateral amygdala; LHA, lateral hypothalamic area; PAG, periaqueductal gray; PF, parafascicular thalamic nucleus; PH, posterior hypothalamic nucleus; RL, rostral linear nucleus raphe; SuM, supramammillary nucleus. Scale bars, 2 mm.

Extended Data Figure 4 | Brain-wide mapping of projections from SuM neurons. a, Coronal sections prepared from a SuM-Cre mouse injected with AAV-DIO-EYFP into the SuM. AcbSh, accumbens nucleus, shell; AHN, anterior hypothalamic nucleus; CM, central medial thalamic nucleus; DG, dentate gyrus; DP, dorsal peduncular cortex; fi, fimbria of hippocampus; IAM, interanteromedial thalamic nucleus; IG, induseum griseum; LHA, lateral hypothalamic area; LHb, lateral habenular nucleus; LPO, lateral preoptic area; LS, lateral septal nucleus; MD, mediodorsal thalamic nucleus; MDl, mediodorsal thalamic nucleus, lateral part; MPO, medial preoptic area; MS, medial septal nucleus; PH, posterior hypothalamic nucleus; RE, nucleus of reuniens; SFi, septofimbrial nucleus; SHi, septohippocampal nucleus; SuM, supramammillary nucleus; vhc, ventral hippocampal commissure. Example is one mouse of four replicates. **b,** Sagittal sections prepared from a SuM-Cre mouse injected with AAV-DIO-EYFP into the SuM. Example shown is one mouse of 3 replicates. Scale bars, 500 μm.

Extended Data Figure 5 | Examination of projections (a) and activity (b) of SuM neurons by clearing and rapid 3D imaging with light sheet microscopy using the Sca*l*eS method. a,

Whole-brain examination of SuM projections. AAV-DIO-EYFP was injected to the SuM of SuM-Cre mice to label SuM projections by Cre-dependent EYFP expression. Acb, accumbens nucleus; DG, dentate gyrus; EC, entorhinal cortex; SuM, supramammillary nucleus. Scales: 14.6 mm (x) × 17.1 mm (y) × 7.5 mm (z) for horizontal views and 11.7 mm (x) × 17.6 mm (y) × 9.0 mm (z) for the sagittal view. One example of 3 replicates is shown. **b**, AbSca*l*e shows EYFP+/c-Fos+ neurons in the SuM after exposure to contextual (left, Mouse #252-1263) or social novelty (right, Mouse #252-1265). 800 μm thick coronal slices were cleared and c-Fos was stained by AbSca*l*e, followed by rapid 3D imaging with laser-scanning confocal microscopy. One example of 3 replicates is shown. Scale bars in the top panel, 1 cm. Scale bars in other panels, 500 μm.

Extended Data Figure 6 | Retrograde tracing of SuM neurons projecting to DG and CA2. a, Collateral projections of DG and CA2-projecting SuM neurons. Dual-color Cre-dependent retrograde AAVs were used to label the cell bodies and axons of SuM neurons projecting to DG (mCherry, red) and CA2 (EYFP, green) (see also Fig. 2d, e). Weak collateral projections from DG and CA2-projecting SuM neurons could be seen in the medial (MS) and lateral septal nucleus (LS) and lateral hypothalamic area (LHA). One example of 6 replicates is shown. Scale bars, 500 μm. **b**, Dual-color cholera toxin subunit B (CTB) labeling was used to trace the cell bodies of SuM neurons projecting to DG (CTB 488, green) and CA2 (CTB 594, red). The majority of the identified SuM cell bodies were found to project solely either to the DG or CA2 with only 2.6 ± 0.5% (N = 3 mice, n = 708 neurons) projecting to both. Scale bars, 250 μm. **c**, **d**, Strategy for multiplex fluorescent in situ hybridization (RNAscope) to identify VGLUT2 and VGAT mRNAs present in the cell bodies of DG- and CA2-projecting SuM neurons. Cre-dependent retrograde AAV was used to label the cell bodies and axons of SuM neurons projecting to DG (**c**) and CA2 (**d**). **e**, **f**, DG- (**e**) and CA2-projecting (**f**) SuM neurons were stained by antisense probes directed against VGLUT2 (570 nm), VGAT (690 nm), and EYFP (520 nm) mRNAs. Scale bars, 500 μm. **g**, **h**, Quantification of EYFP+/VGLUT2+/VGAT+ and EYFP+/VGLUT2+/VGAT- neurons in the DG- (**g**) and CA2-projecting (**h**) SuM neurons. n = 2 animals for each group. All the DG-projecting and CA2-projecting neurons are VGLUT2+. The majority (average: 71.3%, Animal 1: 72.2%, Animal 2: 70.3%) of DG-projecting neurons are

VGAT+, while only a small portion (average: 13.1%, Animal 1: 12.3%, Animal 2: 13.8%) of CA2-projecting neurons are VGAT+.

Extended Data Figure 7 | Validation of the functional segregation of SuM-DG and SuM-CA2 circuits. a, **b**, Strategies of whole-cell voltage clamp recording experiments to validate the physiological segregation of SuM-DG and SuM-CA2 circuits. Retrograde AAV-DIO-ChR2-EYFP was bilaterally injected into the DG (**a**) or CA2 (**b**) of SuM-Cre mice to infect DG- (**a**) or CA2-projecting (**b**) SuM cells. Two weeks later, acute transverse hippocampal slices were prepared and whole-cell voltage clamp recordings were performed in CA2 pyramidal neurons (PNs, **a**) or DG granule cells (GCs, **b**) in order to determine if the DG-projecting SuM neurons also innervated CA2 cells (**a**), and vice versa (**b**). All recorded cells were filled with biocytin for post-hoc identification. Lower panels are confocal images of transverse hippocampal slices recorded with Nissl (blue), ChR2-EYFP expressing SuM fibers (green), and biocytin-filled (red) CA2 PN (**a**) or DG GC (**b**). Scale bars, 250 μm. **c**, **d**, Example light-evoked IPSCs (10 traces, light red; average trace, red) and light-evoked EPSCs (10 traces, grey; average trace, black) recorded with 5 light pulses in CA2 PNs (**c**) and DG GCs (**d**). No inhibitory or excitatory light-evoked current was detected for any of the 17 CA2 PNs from 6 mice and 19 DG GCs from 7 mice, suggesting that DG-projecting SuM cells do not innervate CA2, and vice versa. **e**, **f**, Strategies of behavioral experiments to examine the effect from light bleed-through on the optogenetic dissection of SuM-DG and SuM-CA2 circuits. RetroAAV-DIO-ChR2 was bilaterally injected into the DG (**e**) or CA2 (**f**) of SuM-Cre mice to infect DG- (**e**) or CA2-projecting (**f**) SuM cells. Optic fiber was bilaterally implanted in the uninjected region of each mouse: DG-ChR2 with fibers in CA2 (**e**) or CA2-ChR2 with fibers in DG (**f**). **g–j**, Contextual (**g**, **h**) and social (**i**, **j**) memory tests. Light was delivered to the uninfected region of the hippocampus: DG-ChR2 with light delivery to CA2 (**g**, **i**) or CA2-ChR2 with light delivery to DG (**h**, **j**). Two-way ANOVA with Bonferroni post hoc test, $n = 8$ mice (DG/ChR2) versus $n = 8$ (DG/eYFP) in **g**, $n = 8$ mice (CA2/ChR2) versus $n = 8$ (CA2/eYFP) in **h**. Two-tailed unpaired *t*-tests, $n = 8$ mice (DG/ChR2) versus $n = 8$ (DG/eYFP) in **i**, $n = 8$ mice (CA2/ChR2) versus $n = 8$ (CA2/eYFP) in **j**. n.s., nonsignificant. Error bars show mean ± s.e.m. Boxes denote median (centre line), 25th and 75th percentiles (box edges), and full range of values (whiskers).

Extended Data Figure 8 | Circuit-specific c-Fos mapping and optogenetic identification and recording. **a**, Experimental design to examine the projection specificity of SuM populations that respond to novel contextual or novel social exposure. **b**, **d**, Strategy to label DG- (**b**) or CA2- (**d**) projecting SuM cells using retroAAV-DIO-EYFP with the SuM-Cre mice. **c**, **e**, Images of overlapping populations in the SuM that had contextual or social novelty-induced c-Fos expression and projected to the DG or CA2. On the right of each image is a magnified view of the area within the white box (200 × 200 μm). One example of 3 replicates is shown. **f**, EYFP+/c-Fos+ overlap SuM cell counts for the conditions shown in **c** and **e**. DG-projecting SuM neurons were preferentially activated by contextual novelty (DG-projecting: 53.3 ± 6.1% versus CA2-projecting: 37.1 ± 0.4%, $*P = 0.0429$, one-way ANOVA with Tukey's post hoc test, $n = 3$ mice for both groups), whereas CA2-projecting neurons responded more to social novelty (CA2-projecting: 50.2 ± 1.8% versus DG-projecting: 25.4 ± 2.7%, $**P = 0.0042$, one-way ANOVA with Tukey's post hoc test, $n = 3$ mice for both groups). All error bars show mean ± s.e.m. Open circles are values from individual mice. Scale bars, 200 μm. **g**, **j**, Strategies for optogenetic identification and recording DG- (**g**) and CA2-projecting (**j**) neurons in the SuM. **h**, **k**, Example coronal sections of the SuM with tetrode locations indicated by arrows. Scale bars, 200 μm. **i**, **l**, Histology of recorded animals for circuit-specific optogenetic identification and recording. Reconstructed tetrode tip locations overlaid onto schematic mouse brain slices are shown. Numbers indicate posterior distances from bregma. 35 tetrodes were in target and 8 out of target from 8 mice for recording DG-projecting neurons, while 49 tetrodes were in target and 9 out of target from 11 mice for recording CA2-projecting neurons.

Extended Data Figure 9 | Behavioral tests for contextual memory. a, Familiar (A1-A4 in **b**) and novel contexts (B1 and B2 in **b**) used for contextual memory tests. **b**, Behavioral protocol. **c–e**, Example traveling trajectories of animals during each contextual exposure described in **b** under different optogenetic manipulations of the SuM-DG circuit. **f–i**, Percentage of distances traveled during each contextual exposure under various optogenetic manipulations. Light was delivered in Sessions A4 and B1 to the DG or CA2. The no-light data were used as the control,

in supplementary to the EYFP controls in Fig. 4b–e. Two-way ANOVA with Bonferroni post hoc test, n = 11 mice (DG/ChR2/light) versus n = 11 (DG/ChR2/no light) in **f** (**P = 0.0013, F (20, 100) = 2.882), n = 11 (DG/eNpHR/light) versus n = 11 (DG/eNpHR/no light) in **g** (****P < 0.0001, F (20, 100) = 2.402), n = 11 (CA2/ChR2/light) versus n = 11 (CA2/ChR2/no light) in **h**, n = 10 (CA2/eNpHR/light) versus n = 10 (CA2/eNpHR/no light) in **i**. All error bars show mean ± s.e.m.

Extended Data Figure 10 | Synaptic transmission from SuM terminals to DG granule cells (GCs) and CA2 pyramidal neurons (PNs). **a**, Identification of direct glutamatergic transmission in CA2 from SuM inputs. (left) Diagram illustrating the whole-cell recordings of hippocampal pyramidal neurons (PNs) and SuM fiber stimulation in acute slice preparation. Cesium-based intracellular solution was used in the recording pipette and all cells were recorded in voltage-clamp mode with a membrane potential held at -70 mV in order to record excitatory glutamatergic transmission. (right) Diagram mapping the location of all PNs recorded in the hippocampus with closed circles indicating connected cells and open circles indicating unconnected cells with no detected transmission. Cells were classified as CA1 (n = 11, all unconnected), CA2 (n = 46 connected, n = 30 unconnected) and CA3 (n = 19 connected, n = 29 unconnected) based on morphology (the presence of thorny excrecsences for CA3) and location. Circle color indicates cell type with CA2 PNs black, CA3 PNs brown and CA1 PNs orange. **b**, Identification of feed-forward inhibitory transmission in CA2 from SuM inputs. (left) Diagram illustrating the local circuitry involved in the feed-forward inhibition recruited by SuM inputs in the hippocampus. The same recording configuration was used as shown in **a**, except that cells were held at +10 mV in order to measure feed-forward inhibitory transmission. (right) Diagram mapping PNs in the hippocampus that receive feed-forward transmission from light-evoked SuM inputs with unconnected cells shown as open circles and connected cells as filled circles. No CA1 PNs received feed-forward inhibition (n = 11) while over half of CA2 PNs received detectable feed-forward inhibition (n = 30 connected, n = 18 unconnected) as well as a fraction of CA3 PNs (n = 20 connected, n = 18 unconnected). **c**, Identification of excitatory and inhibitory transmission to DG granule cells (GCs) from SuM inputs. (left) Diagram illustrating the experimental setup to measure local excitatory and inhibitory circuitry recruited by SuM

inputs in the DG. The same recording configuration was used as shown in **a** and **b**. Cells were held at -70 mV to measure excitatory transmission and then at +10 mV. Inhibitory transmission was measured before and after the addition of 10 μM NBQX & 50 μM APV to distinguish feed-forward and direct inhibitory transmission. (right) Diagram mapping GCs in the DG that receive excitatory and inhibitory (both feed-forward and direct) transmission from light-evoked SuM inputs. Blue filled circles mark the location of cells that received both excitatory and inhibitory transmission (n = 21). All cells received both direct and feed-forward inhibition. Yellow-filled circles mark cells that did not receive detectable excitatory transmission, but both direct and feed-forward inhibitory transmission (n = 3). Data for panels **a.-c.** were collected from 156 slices from 92 mice. Abbreviations: so, stratum oriens; sp, stratum pyramidale; sr, stratum radiatum; mf, mossy fiber; ml, molecular layer; gcl, granule cell layer. **d**, Inverted epifluorescent image of a hippocampal slice with a DG GC and a CA2 PN. Each neuron had been recorded and filled with biocytin which was stained with streptavidin-conjugated fluorophore. **e**, Dendritic (blue) and axonal (red) reconstruction of the cells in **d** with the hippocampal regions demarcated. **f**, Diagram illustrating the local circuitry and whole-cell recording configuration of DG GCs in acute brain slices prepared from SuM-Cre mice injected with AAV-DIO-ChR2-EYFP. SuM axonal terminals were illuminated by a 0.5 ms 488 nm light stimulation. IN, interneuron. **g**, Sample traces of light-evoked EPSCs recorded at −70 mV (individual traces in grey, average trace in black) and IPSCs recorded at +10 mV (individual traces in light red, average trace in red) in a same DG GC under voltage clamp. The blue line denotes when the light stimulus was applied. **h**, Normalized cumulative distribution of latencies for DG GC EPSCs (black) and IPSCs (red), both displaying response latencies consistent with direct monosynaptic transmission (4.1 ± 0.3 ms for EPSCs, n = 20 GCs; 4.16 ± 0.3 ms for IPSCs, n = 22 GCs; Student's t-test, P = 0.94; Kolmogorov–Smirnov test, P = 0.97). **i**, **j**, Sample traces (**i**) and time course of amplitudes (**j**, IPSCs only, n = 22 GCs from 8 mice) of light-evoked EPSCs (black) and IPSCs (red) recorded in DG GCs before and after application of 10 μM NBQX & 50 μM APV (grey), and further application of 1 μM SR95531 & 2 μM CGP55845A (green). AMPA and NMDA receptor blockers completely blocked EPSCs (13 ± 3.1 pA, n = 20 GCs), but only partially blocked IPSCs (by 36%, 86 ± 21 pA before, 31 ± 7.2 pA following NBQX and APV addition, $^{**}P$ =0.0037, Wilcoxon signed-rank test, n = 22 GCs from 8 mice), indicating that there is feed-forward inhibition recruited by SuM inputs, accompanied by a larger amount of direct inhibitory

transmission. The remaining light-evoked IPSCs were entirely blocked by the subsequent addition of GABAA and GABAB receptor blockers, suggesting that DG-projecting neurons in the SuM are capable of simultaneously releasing both glutamate and GABA. **k**, Diagram similar to **f**, showing the local circuitry and whole-cell recording configuration of CA2 PNs. **l**, Sample traces of EPSCs recorded at −70 mV (individual traces in grey, average trace in black) and IPSCs recorded at +10 mV (individual traces in light red, average trace in red) in a same CA2 PN under voltage clamp. Note the increased latency of IPSCs onset compared to EPSCs. **m**, Normalized cumulative distribution of latencies for CA2 PN EPSCs (black) and IPSCs (red). IPSCs displayed significantly different response latencies from the EPSCs, with a longer IPSC response latency consistent with bi-synaptic feed-forward inhibition (2.9 ± 0.1 ms for EPSCs, n = 166 PNs; 6.2 ± 0.4 ms for IPSCs, n = 69 PNs; ****$P < 0.0001$, Mann–Whitney U test; Kolmogorov–Smirnov test, ****$P < 0.0001$, data from 92 mice). **n**, **o**, Sample traces (**n**) and time course of amplitudes (**o**, IPSCs only, n = 7 from 4 mice) of light-evoked EPSCs (black) and IPSCs (red) recorded in CA2 PNs before and after application of 10 μM NBQX & 50 μM APV (grey). Both the EPSCs (16 ± 4.8 pA, n = 6 PNs from 4 mice) and IPSCs (167 ± 40 pA, n = 7 PNs from 4 mice) were completely blocked by the application of AMPA and NMDA receptor blockers, indicating that the synaptic transmission from the SuM is entirely glutamatergic in CA2. Notably, both SuM-DG and SuM-CA2 transmissions recruit a robust feed-forward inhibition. **p**, Confirmation of SuM-CA2 transmission by the addition of tetrodotoxin (TTX) and 4-aminopyridine (4-AP) to isolate transmitter release resulting from direct optical terminal depolarization. Application of TTX & 4-AP abolishes IPSCs and spares EPSCs in CA2 pyramidal neurons (PNs), consistent with mono-synaptic excitation and di-synaptic inhibition. Control sample traces are shown in black (EPSC) and red (IPSC), while traces following application of TTX & 4-AP are shown in grey. **q**, Time course of light-evoked EPSC and IPSC amplitudes upon application of 0.2 μM TTX & 100 μM 4-AP in which a longer light stimulus was used to directly depolarize the SuM axonal terminal. Initial amplitudes were 20.2 ± 6.1 pA for EPSCs and 110 ± 50 pA for IPSCs, and 9.3 ± 7.7 pA for EPSCs and 4.8 ± 0.7 pA for IPSCs following TTX & 4-AP, indicating a 61 ± 24 % block of EPSCs and 88 ± 4.2 % block of IPSCs by TTX & 4-AP. P = 0.22 for EPSCs, P = 0.016 for IPSCs, Wilcoxon signed-rank test, n = 7 PNs from 3 mice. All error bars show mean ± s.e.m.

Extended Data Figure 11 | Retrograde tracing of upstream inputs to the DG- and CA2-projecting SuM neurons. a, **b**, Strategies of projection-specific retrograde tracing to map the upstream inputs to the DG- (**a**) and CA2-projecting (**b**) neurons. Retrograde AAV helper viruses expressing the rabies G protein and the TVA receptor are injected into DG (**a**) or into CA2 (**b**), and three weeks later EnvA pseudotyped rabies virus expressing mCherry is injected into the SuM. This allows for the retrograde labeling of upstream neurons that send efferent axons to DG- or CA2-projecting SuM cells by the rabies virus. **c**, **d**, Coronal sections showing DG- (**c**) and CA2-projecting (**d**) starter cells in the SuM. Cells in red (mCherry) are TVA+ cells that express rabies virus (one example of four mice for DG injections, one example of five mice for CA2 injections). Cells in green (GFP) express oG (optimized glycoprotein). The mCherry+/GFP+ overlapping cells (yellow) are starter cells where the *trans*-complementation of RV*dG* with oG results in the production of oG+RV*dG* that spreads trans-synaptically to input cells. Scale bar, 1 mm. **e**, **f**, Coronal sections with trans-synaptically labeled input cells upstream to the DG- (**e**) and CA2-projecting (**f**) SuM neurons. Scale bars, 1 mm. **g**, **h**, Quantification of inputs from various brain regions to the DG- (**g**, $n = 4$ mice) and CA2-projecting (**h**, $n = 5$ mice) SuM neurons. Both populations received extensive inputs from subcortical regions including the hypothalamus, brainstem, septum and nucleus accumbens. However, the inputs to the DG-projecting population were comparatively biased to brain regions in the reward and motor systems, such as the VTA, SI, AcbSh, LS and MS, while the CA2 projectors received proportionally greater inputs from neurons in socially engaged regions, particularly the PVH (*$P = 0.0159$, Mann-Whitney U test) and MPO. All error bars show mean ± s.e.m. LS, lateral septal nucleus; MS, medial septal nucleus; SI, substantia innominata; AcbSh, accumbens nucleus, shell; ZI, zona incerta; LHA, lateral hypothalamic area; MPO, medial preoptic area; LPO, lateral preoptic area; PVH, paraventricular hypothalamic nucleus; PH, posterior hypothalamic nucleus; PAG, periaqueductal gray; MRN, midbrain reticular nucleus; VTA, ventral tegmental area; Raphe: DR, dorsal raphe nucleus & MnR, median raphe nucleus.

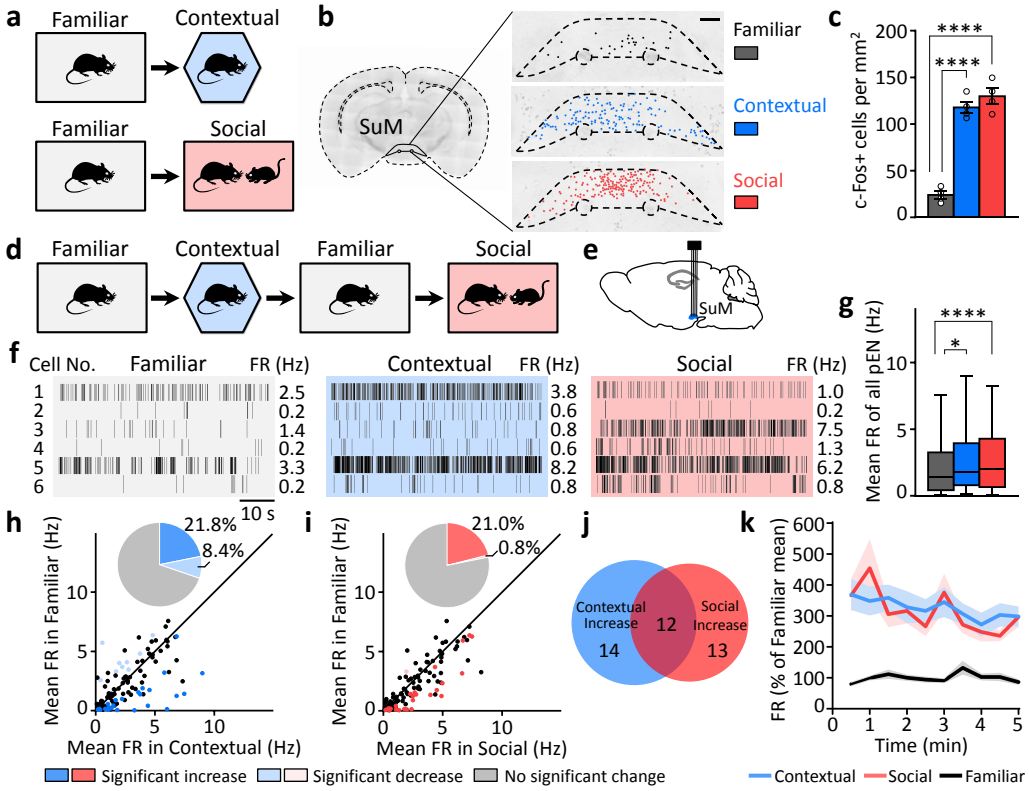
a
Familiar
Contextual
Familiar
Social
b
SuM
Familiar
Contextual
Social
c
c-Fos+ cells per mm2
****
****
d
Familiar
Contextual
Familiar
Social
e
SuM
f
Cell No.
Familiar
FR (Hz)
Contextual
FR (Hz)
Social
FR (Hz)
10 s
g
Mean FR of all pEN (Hz)
****
*
h
21.8%
8.4%
Mean FR in Familiar (Hz)
Mean FR in Contextual (Hz)
i
21.0%
0.8%
Mean FR in Familiar (Hz)
Mean FR in Social (Hz)
j
Contextual Increase
14
12
Social Increase
13
k
FR (% of Familiar mean)
Time (min)
Significant increase
Significant decrease
No significant change
Contextual
Social
Familiar

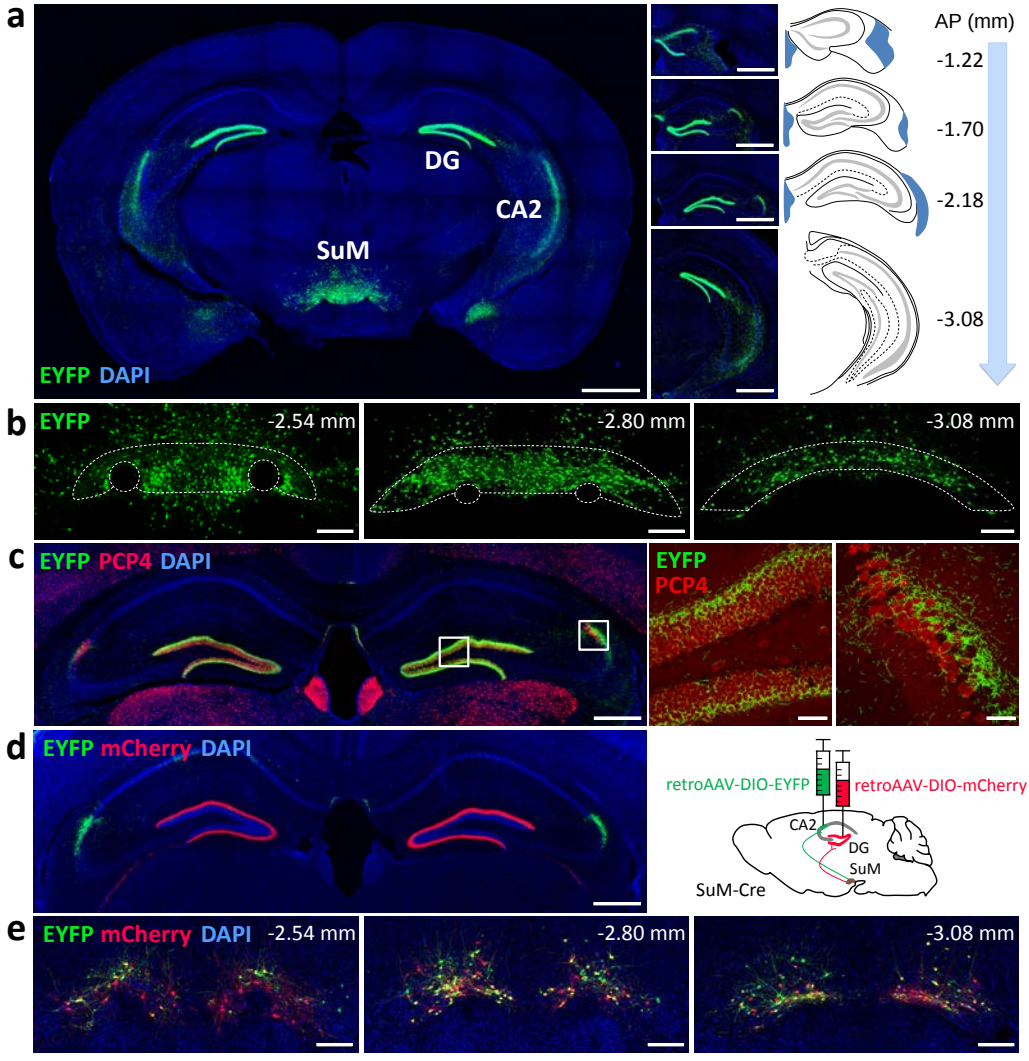
a
DG
CA2
SuM
EYFP DAPI
AP (mm)
-1.22
-1.70
-2.18
-3.08
b
EYFP
-2.54 mm
-2.80 mm
-3.08 mm
c
EYFP PCP4 DAPI
EYFP
PCP4
d
EYFP mCherry DAPI
retroAAV-DIO-EYFP
retroAAV-DIO-mCherry
CA2
DG
SuM
SuM-Cre
e
EYFP mCherry DAPI
-2.54 mm
-2.80 mm
-3.08 mm

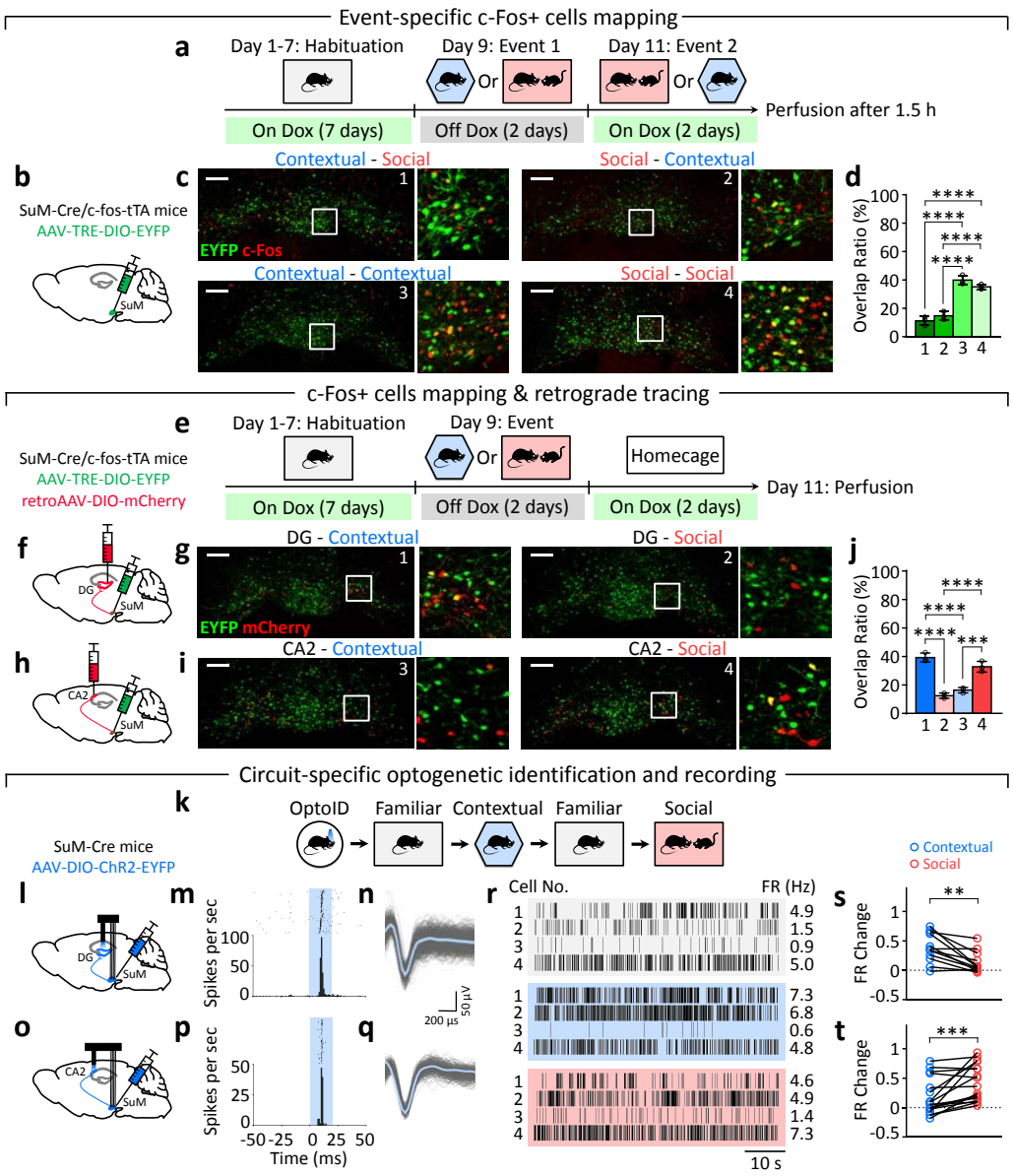
Event-specific c-Fos+ cells mapping
a
Day 1-7: Habituation
Day 9: Event 1
Or
Day 11: Event 2
Or
Perfusion after 1.5 h
On Dox (7 days)
Off Dox (2 days)
On Dox (2 days)
b
SuM-Cre/c-fos-tTA mice
AAV-TRE-DIO-EYFP
SuM
c
Contextual - Social
Social - Contextual
Contextual - Contextual
Social - Social
EYFP c-Fos
1
2
3
4
d
Overlap Ratio (%)
****
c-Fos+ cells mapping & retrograde tracing
e
SuM-Cre/c-fos-tTA mice
AAV-TRE-DIO-EYFP
retroAAV-DIO-mCherry
Day 1-7: Habituation
Day 9: Event
Or
Homecage
Day 11: Perfusion
On Dox (7 days)
Off Dox (2 days)
On Dox (2 days)
f
DG
SuM
g
DG - Contextual
DG - Social
EYFP mCherry
h
CA2
SuM
i
CA2 - Contextual
CA2 - Social
j
Overlap Ratio (%)
****
***
Circuit-specific optogenetic identification and recording
k
OptoID
Familiar
Contextual
Familiar
Social
SuM-Cre mice
AAV-DIO-ChR2-EYFP
l
DG
SuM
m
Spikes per sec
n
200 µs
50 µV
o
CA2
SuM
p
Spikes per sec
Time (ms)
q
r
Cell No.
FR (Hz)
4.9
1.5
0.9
5.0
7.3
6.8
0.6
4.8
4.6
4.9
1.4
7.3
10 s
Contextual
Social
s
FR Change
**
t
FR Change
***

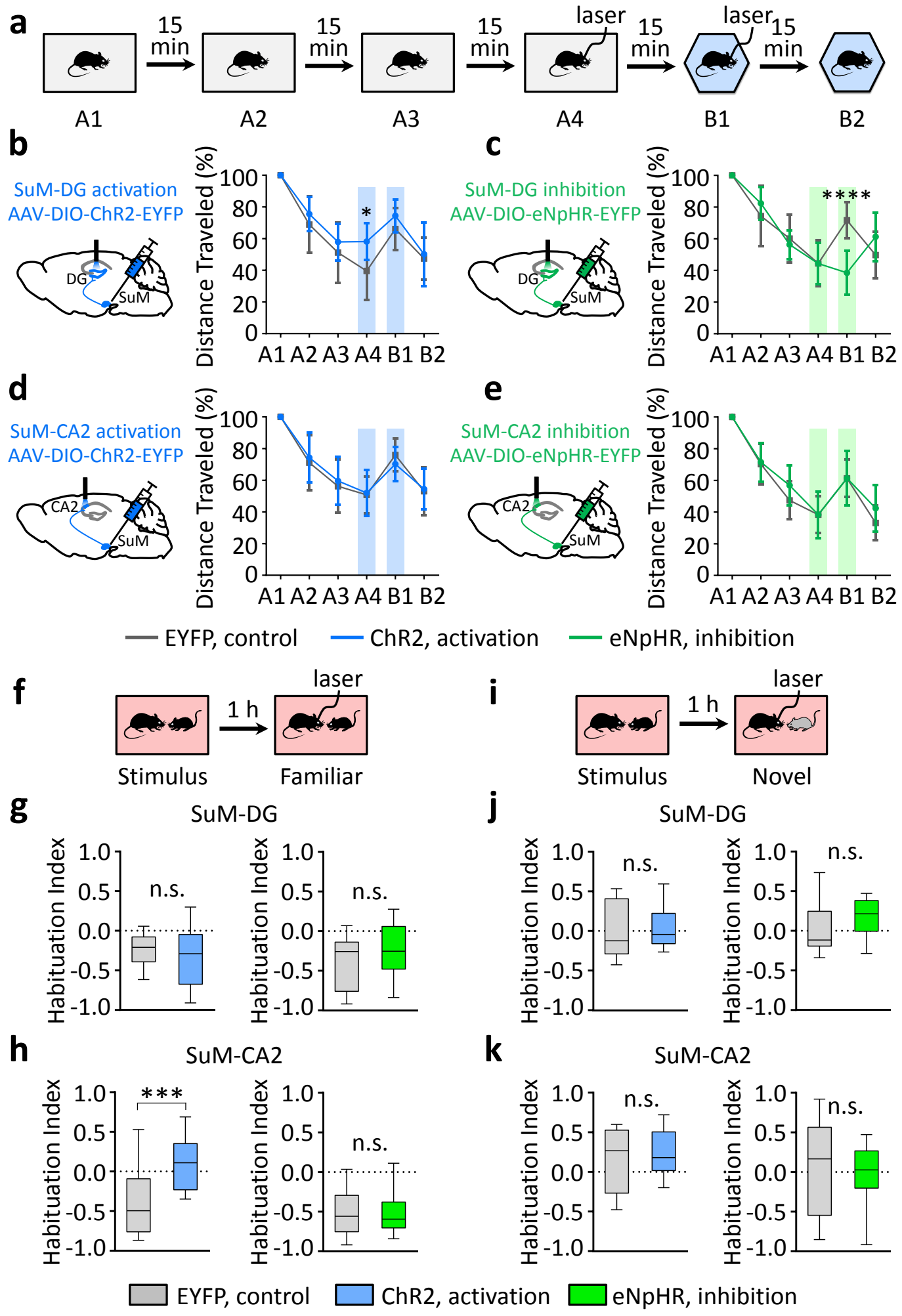
a
15 min
laser
A1
A2
A3
A4
B1
B2
b
SuM-DG activation
AAV-DIO-ChR2-EYFP
DG
SuM
Distance Traveled (%)
c
SuM-DG inhibition
AAV-DIO-eNpHR-EYFP
****
d
SuM-CA2 activation
AAV-DIO-ChR2-EYFP
CA2
e
SuM-CA2 inhibition
AAV-DIO-eNpHR-EYFP
EYFP, control
ChR2, activation
eNpHR, inhibition
f
1 h
Stimulus
Familiar
i
Novel
g
SuM-DG
Habituation Index
n.s.
j
h
SuM-CA2
***
k
EYFP, control
ChR2, activation
eNpHR, inhibition

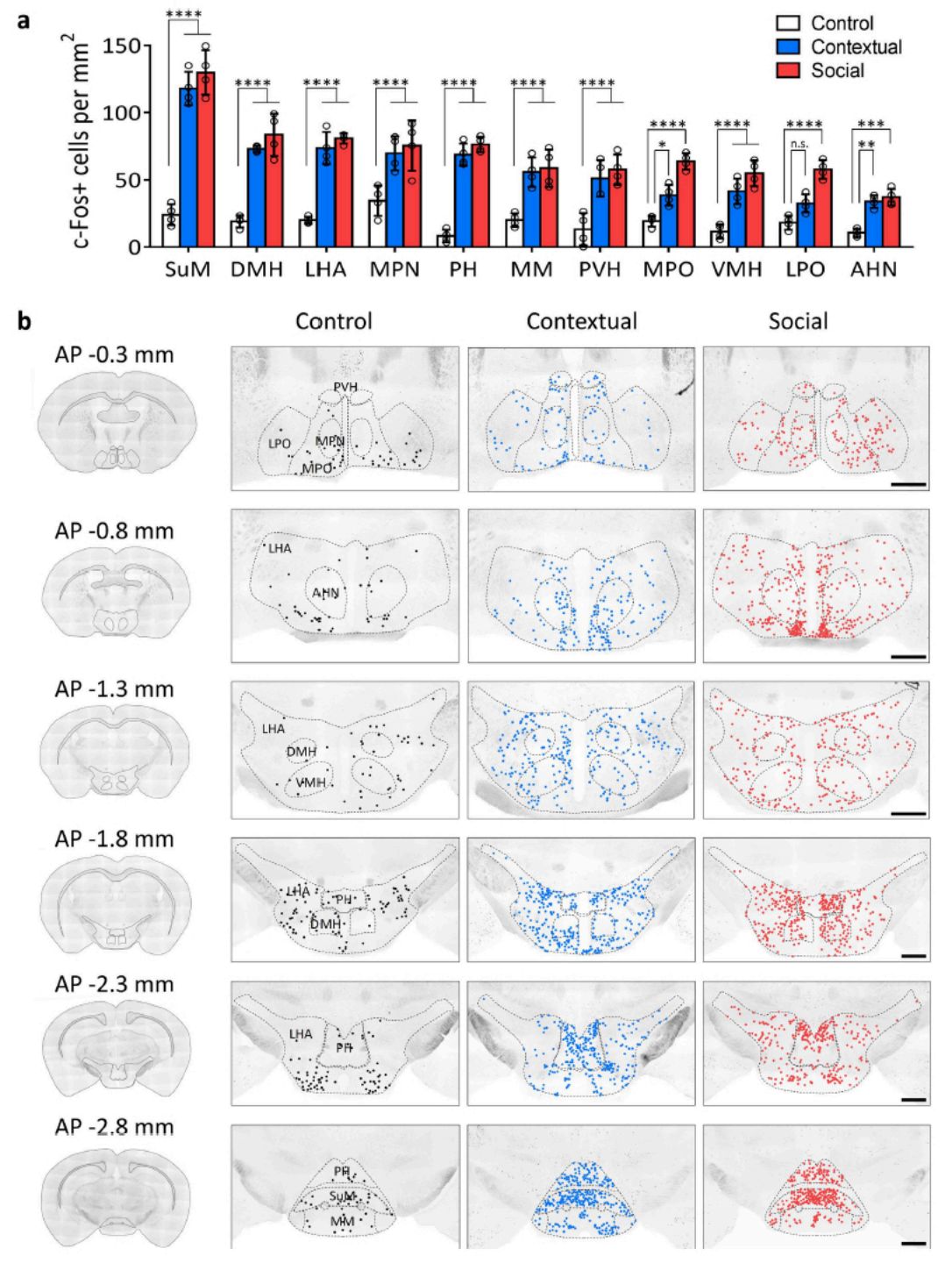
a
c-Fos+ cells per mm2
150
100
50
0
Control
Contextual
Social
****
*
n.s.
**
***
SuM
DMH
LHA
MPN
PH
MM
PVH
MPO
VMH
LPO
AHN
b
Control
Contextual
Social
AP -0.3 mm
PVH
LPO
MPN
MPO
AP -0.8 mm
LHA
AHN
AP -1.3 mm
LHA
DMH
VMH
AP -1.8 mm
LHA
PH
DMH
AP -2.3 mm
LHA
PH
AP -2.8 mm
PH
SuM
MM

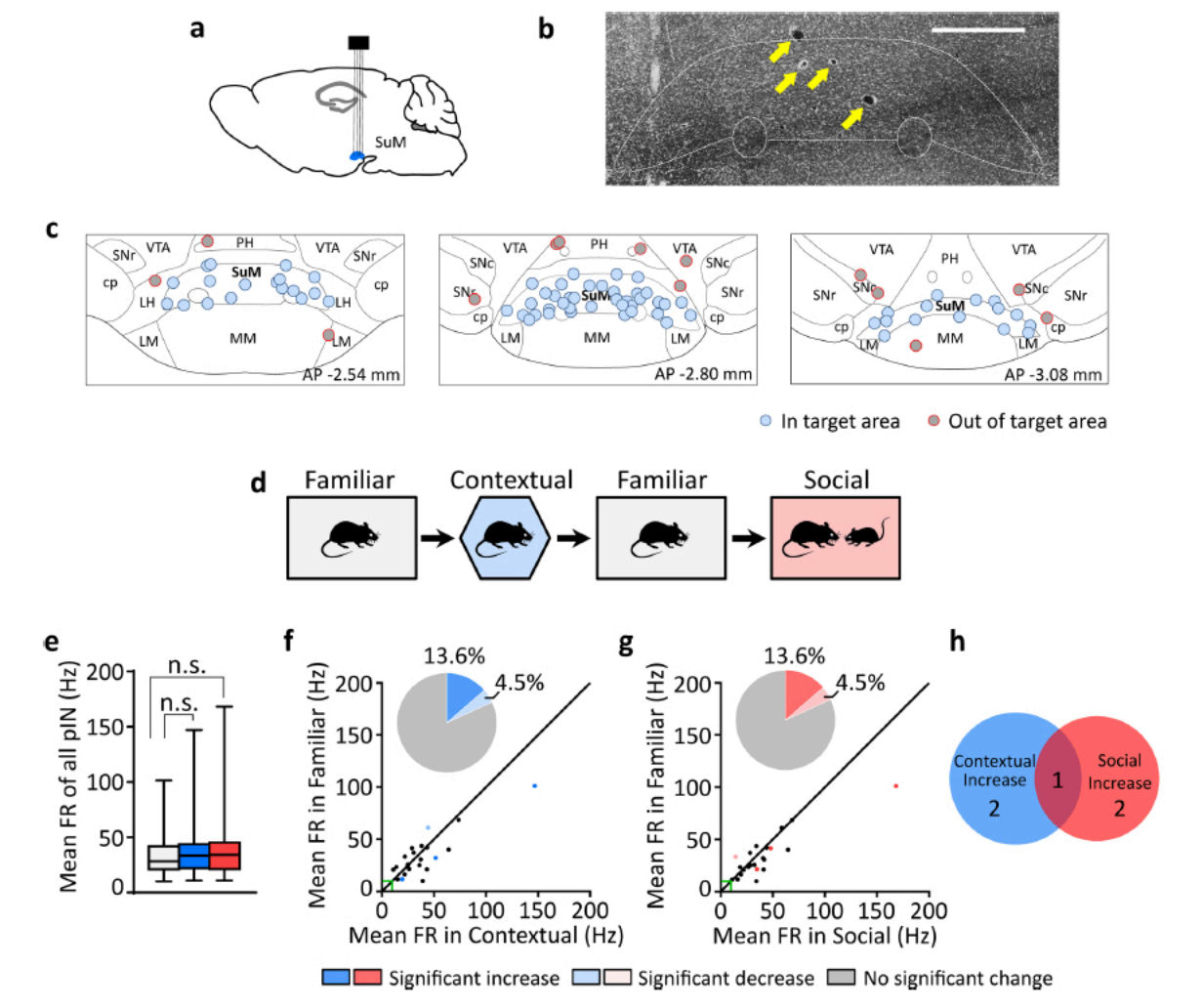
a
SuM
b
c
SNr
VTA
PH
VTA
SNr
cp
SuM
LH
LH
cp
LM
MM
LM
AP -2.54 mm
SNc
VTA
PH
VTA
SNc
SNr
SuM
SNr
cp
cp
LM
MM
LM
AP -2.80 mm
VTA
VTA
PH
SNr
SNc
SNc
SNr
SuM
cp
cp
LM
MM
LM
AP -3.08 mm
In target area
Out of target area
d
Familiar
Contextual
Familiar
Social
e
Mean FR of all pIN (Hz)
200
150
100
50
0
n.s.
n.s.
f
13.6%
4.5%
Mean FR in Familiar (Hz)
Mean FR in Contextual (Hz)
0
50
100
150
200
g
13.6%
4.5%
Mean FR in Familiar (Hz)
Mean FR in Social (Hz)
h
Contextual Increase
2
1
Social Increase
2
Significant increase
Significant decrease
No significant change

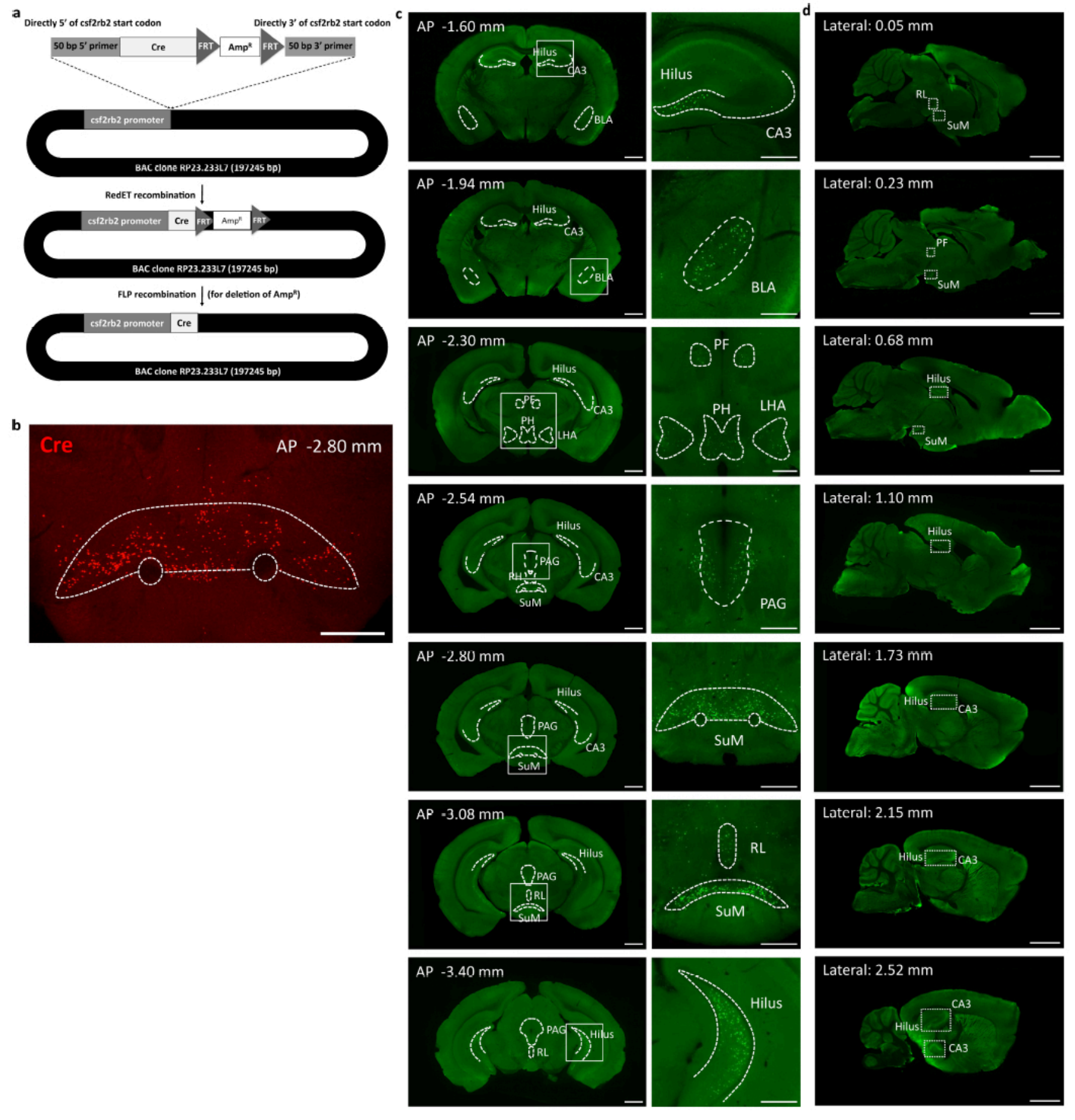
a
Directly 5′ of csf2rb2 start codon
Directly 3′ of csf2rb2 start codon
50 bp 5′ primer
Cre
FRT
Amp^R
FRT
50 bp 3′ primer
csf2rb2 promoter
BAC clone RP23.233L7 (197245 bp)
RedET recombination
csf2rb2 promoter
Cre
FRT
Amp^R
FRT
BAC clone RP23.233L7 (197245 bp)
FLP recombination
(for deletion of Amp^R)
csf2rb2 promoter
Cre
BAC clone RP23.233L7 (197245 bp)
b
Cre
AP -2.80 mm
c
AP -1.60 mm
Hilus
CA3
BLA
Hilus
CA3
AP -1.94 mm
Hilus
CA3
BLA
BLA
AP -2.30 mm
Hilus
PF
PH
CA3
LHA
PF
PH
LHA
AP -2.54 mm
Hilus
PAG
RL
CA3
SuM
PAG
AP -2.80 mm
Hilus
PAG
CA3
SuM
SuM
AP -3.08 mm
Hilus
PAG
RL
SuM
RL
SuM
AP -3.40 mm
PAG
RL
Hilus
Hilus
d
Lateral: 0.05 mm
RL
SuM
Lateral: 0.23 mm
PF
SuM
Lateral: 0.68 mm
Hilus
SuM
Lateral: 1.10 mm
Hilus
Lateral: 1.73 mm
Hilus
CA3
Lateral: 2.15 mm
Hilus
CA3
Lateral: 2.52 mm
CA3
Hilus
CA3

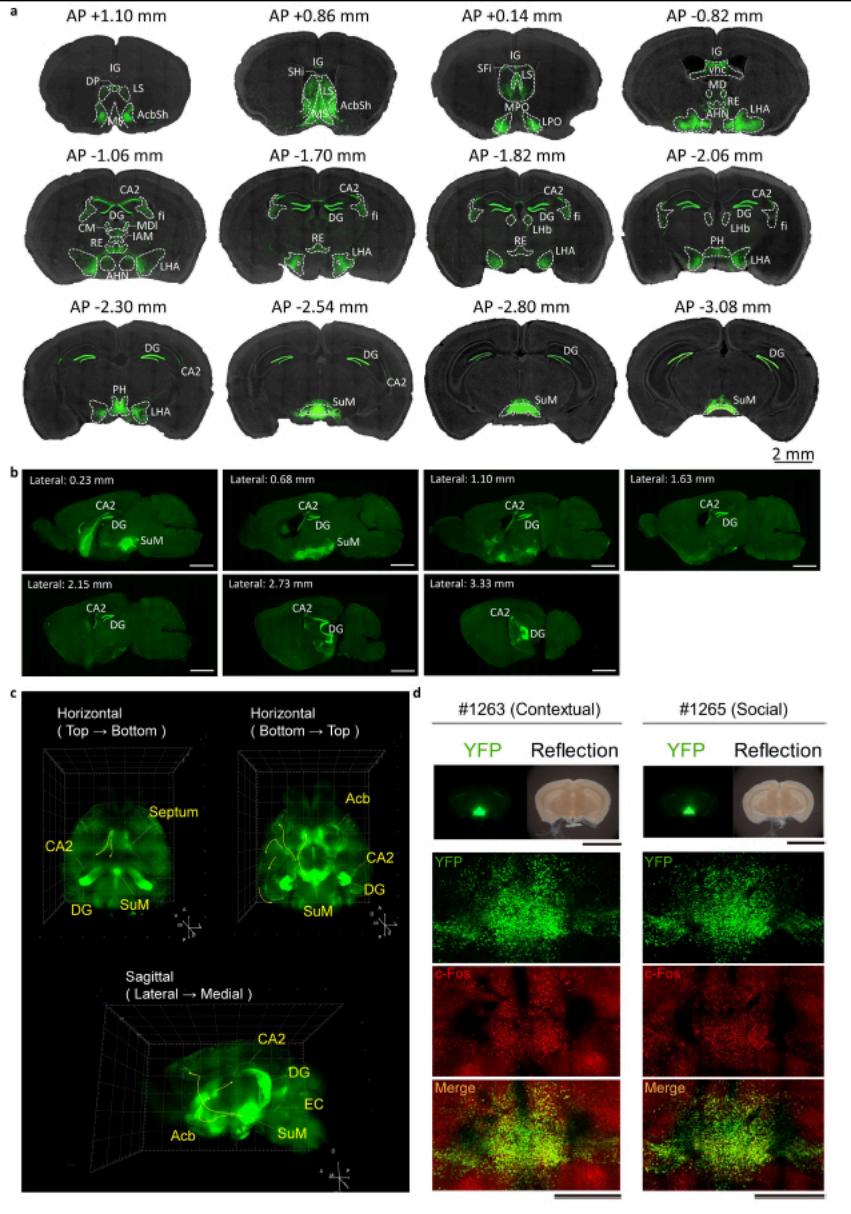
a
AP +1.10 mm
IG
DP
LS
AcbSh
MS
AP +0.86 mm
IG
SHi
LS
AcbSh
MS
AP +0.14 mm
IG
SFi
LS
MPO
LPO
AP -0.82 mm
IG
Vhc
MD
RE
AFN
LHA
AP -1.06 mm
CA2
DG
fi
CM
MDl
IAM
RE
AHN
LHA
AP -1.70 mm
CA2
DG
fi
RE
LHA
AP -1.82 mm
CA2
DG
fi
LHb
RE
LHA
AP -2.06 mm
CA2
DG
fi
LHb
PH
LHA
AP -2.30 mm
DG
CA2
PH
LHA
AP -2.54 mm
DG
CA2
SuM
AP -2.80 mm
DG
SuM
AP -3.08 mm
DG
SuM
2 mm
b
Lateral: 0.23 mm
CA2
DG
SuM
Lateral: 0.68 mm
CA2
DG
SuM
Lateral: 1.10 mm
CA2
DG
Lateral: 1.63 mm
CA2
DG
Lateral: 2.15 mm
CA2
DG
Lateral: 2.73 mm
CA2
DG
Lateral: 3.33 mm
CA2
DG
c
Horizontal
(Top → Bottom)
Septum
CA2
DG
SuM
Horizontal
(Bottom → Top)
Acb
CA2
DG
SuM
Sagittal
(Lateral → Medial)
CA2
DG
EC
Acb
SuM
d
#1263 (Contextual)
#1265 (Social)
YFP
Reflection
YFP
Reflection
YFP
c-Fos
Merge
YFP
c-Fos
Merge

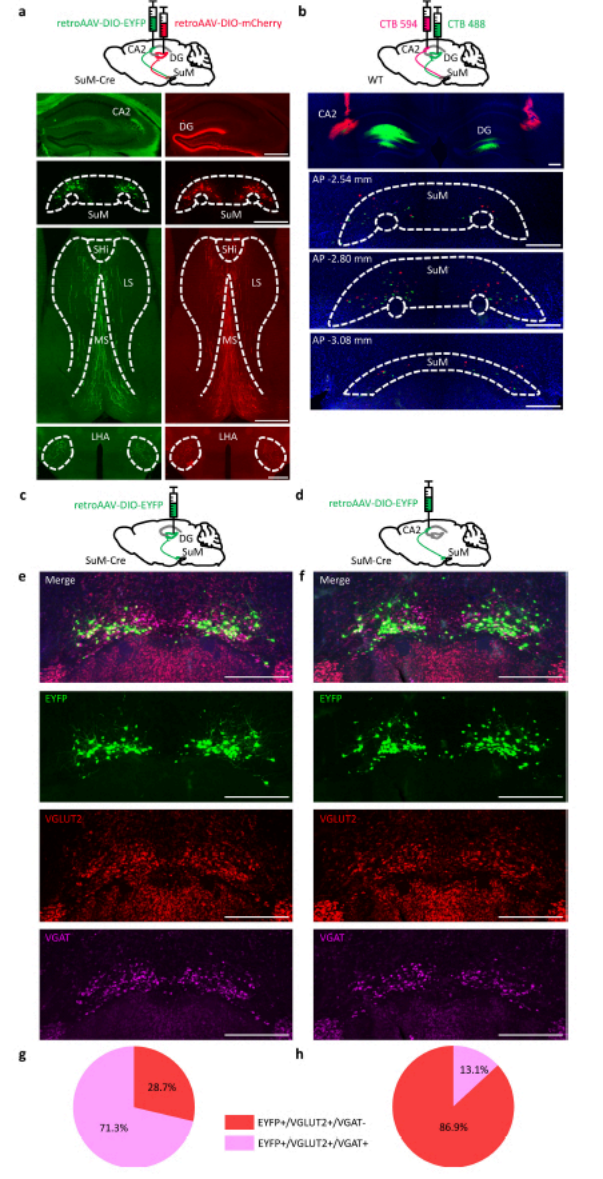
a
retroAAV-DIO-EYFP
retroAAV-DIO-mCherry
CA2
DG
SuM
SuM-Cre
CA2
DG
SuM
SuM
SHi
LS
MS
LHA
b
CTB 594
CTB 488
CA2
DG
SuM
WT
CA2
DG
AP -2.54 mm
SuM
AP -2.80 mm
SuM
AP -3.08 mm
SuM
c
retroAAV-DIO-EYFP
DG
SuM
SuM-Cre
d
retroAAV-DIO-EYFP
CA2
SuM
SuM-Cre
e
Merge
EYFP
VGLUT2
VGAT
f
Merge
EYFP
VGLUT2
VGAT
g
28.7%
71.3%
EYFP+/VGLUT2+/VGAT-
EYFP+/VGLUT2+/VGAT+
h
13.1%
86.9%

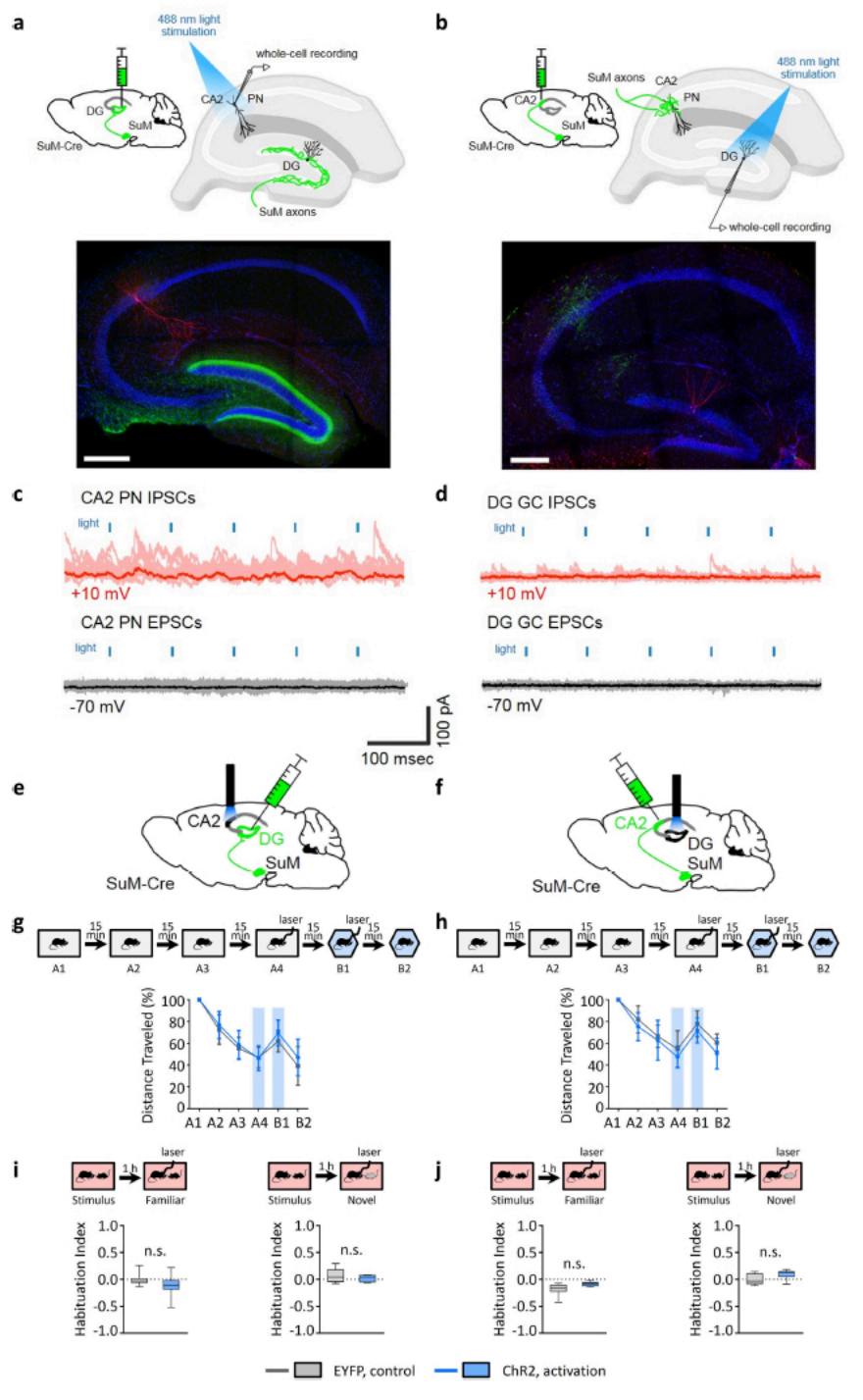
a
488 nm light stimulation
whole-cell recording
DG
SuM
SuM-Cre
CA2
PN
DG
SuM axons
b
SuM axons
CA2
488 nm light stimulation
PN
CA2
SuM
SuM-Cre
DG
whole-cell recording
c
CA2 PN IPSCs
light
+10 mV
CA2 PN EPSCs
light
-70 mV
100 pA
100 msec
d
DG GC IPSCs
light
+10 mV
DG GC EPSCs
light
-70 mV
e
CA2
DG
SuM
SuM-Cre
f
CA2
DG
SuM
SuM-Cre
g
15 min
laser
A1 A2 A3 A4 B1 B2
Distance Traveled (%)
A1 A2 A3 A4 B1 B2
h
15 min
laser
A1 A2 A3 A4 B1 B2
Distance Traveled (%)
A1 A2 A3 A4 B1 B2
i
1 h
laser
Stimulus
Familiar
Habituation Index
n.s.
Stimulus
Novel
Habituation Index
n.s.
j
1 h
laser
Stimulus
Familiar
Habituation Index
n.s.
Stimulus
Novel
Habituation Index
n.s.
EYFP, control
ChR2, activation

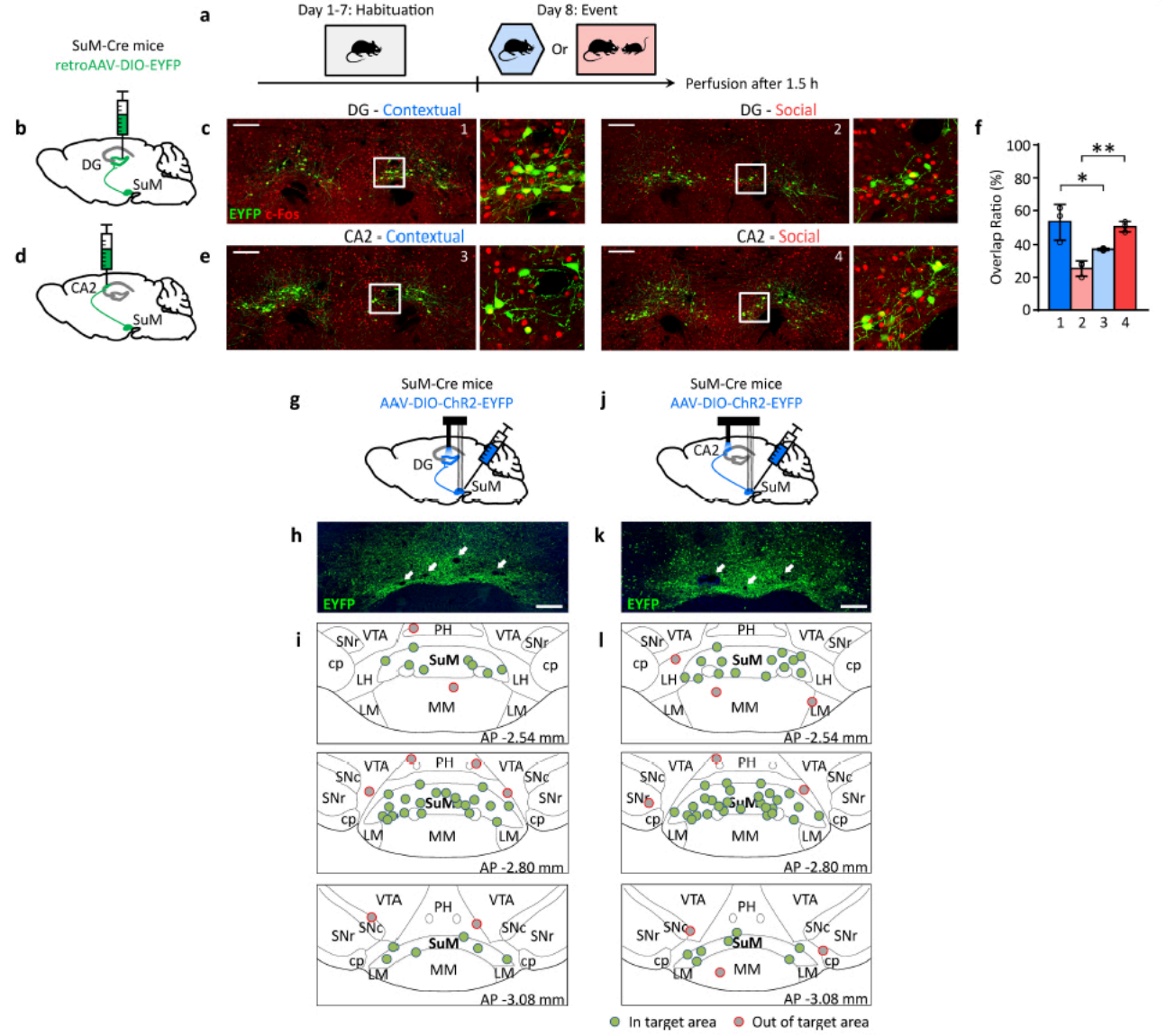
c-Fos+ cells mapping & retrograde tracing
a
Day 1-7: Habituation
Day 8: Event
Or
Perfusion after 1.5 h
SuM-Cre mice
retroAAV-DIO-EYFP
b
DG
SuM
d
CA2
SuM
c
DG - Contextual
DG - Social
1
2
EYFP c-Fos
e
CA2 - Contextual
CA2 - Social
3
4
f
Overlap Ratio (%)
100
80
60
40
20
0
1 2 3 4
*
**
g
SuM-Cre mice
AAV-DIO-ChR2-EYFP
DG
SuM
j
SuM-Cre mice
AAV-DIO-ChR2-EYFP
CA2
SuM
h
EYFP
k
EYFP
i
l
SNr VTA PH VTA SNr
cp
SuM
LH LH
LM MM LM
AP -2.54 mm
SNc VTA PH VTA SNc
SNr SNr
cp cp
SuM
LM MM LM
AP -2.80 mm
VTA PH VTA
SNc SNc
SNr SNr
cp cp
SuM
LM MM LM
AP -3.08 mm
In target area
Out of target area

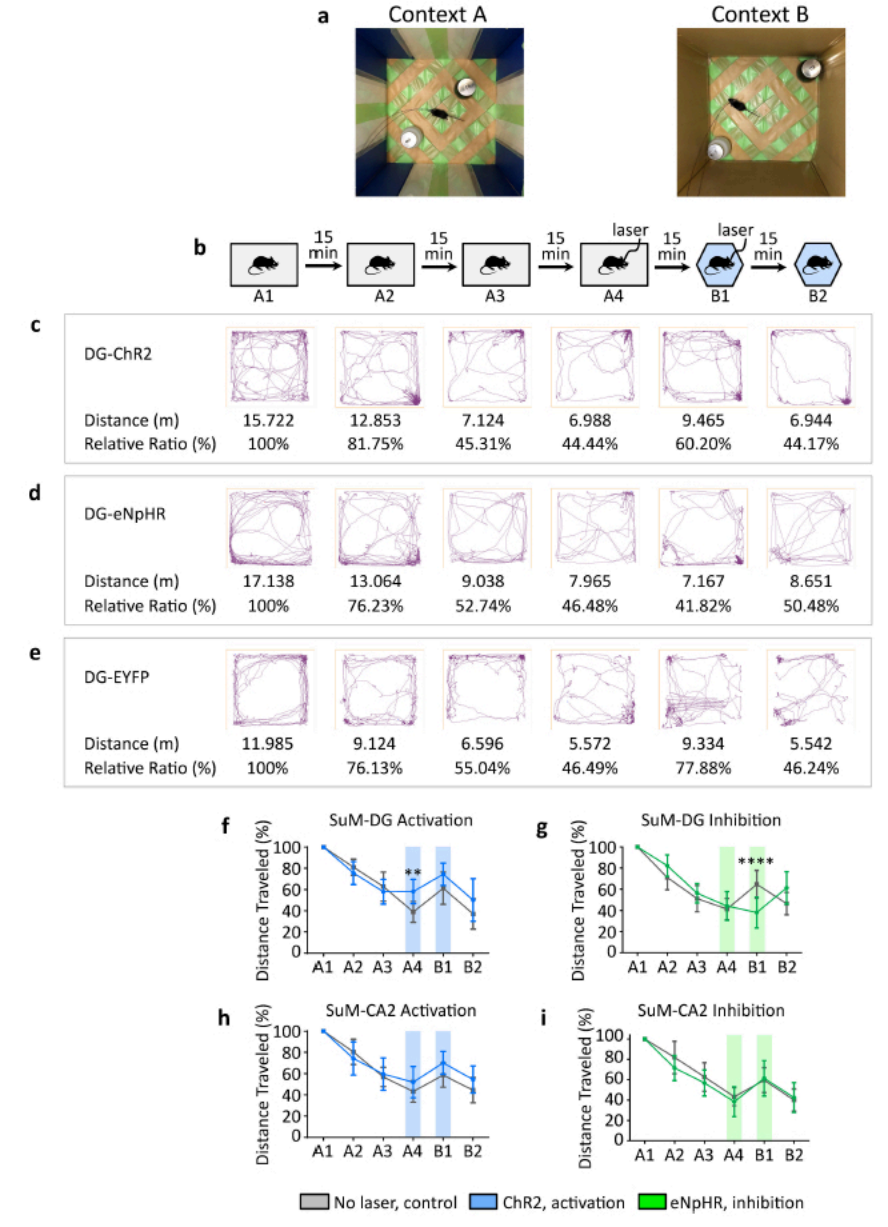
a
Context A
Context B
b
15 min
laser
A1
A2
A3
A4
B1
B2
c
DG-ChR2
Distance (m) 15.722 12.853 7.124 6.988 9.465 6.944
Relative Ratio (%) 100% 81.75% 45.31% 44.44% 60.20% 44.17%
d
DG-eNpHR
Distance (m) 17.138 13.064 9.038 7.965 7.167 8.651
Relative Ratio (%) 100% 76.23% 52.74% 46.48% 41.82% 50.48%
e
DG-EYFP
Distance (m) 11.985 9.124 6.596 5.572 9.334 5.542
Relative Ratio (%) 100% 76.13% 55.04% 46.49% 77.88% 46.24%
f
SuM-DG Activation
g
SuM-DG Inhibition
h
SuM-CA2 Activation
i
SuM-CA2 Inhibition
Distance Traveled (%)
**
****
No laser, control
ChR2, activation
eNpHR, inhibition

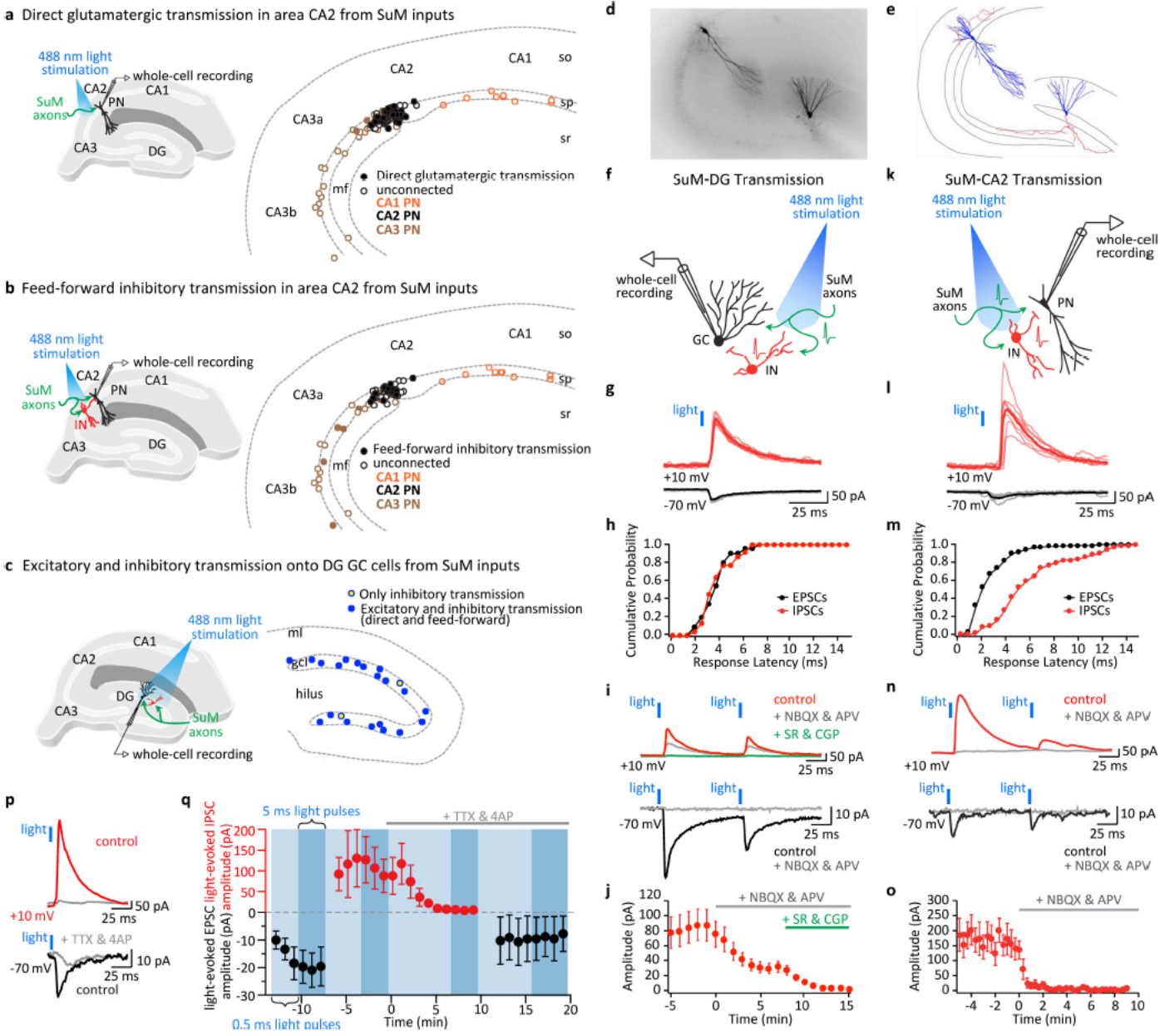
a Direct glutamatergic transmission in area CA2 from SuM inputs
488 nm light stimulation
whole-cell recording
SuM axons
CA2
CA1
PN
CA3
DG
so
sp
sr
CA3a
CA3b
mf
Direct glutamatergic transmission
unconnected
CA1 PN
CA2 PN
CA3 PN
b Feed-forward inhibitory transmission in area CA2 from SuM inputs
IN
Feed-forward inhibitory transmission
c Excitatory and inhibitory transmission onto DG GC cells from SuM inputs
Only inhibitory transmission
Excitatory and inhibitory transmission (direct and feed-forward)
ml
gcl
hilus
d
e
f SuM-DG Transmission
GC
k SuM-CA2 Transmission
g
l
light
+10 mV
-70 mV
50 pA
25 ms
h
m
Cumulative Probability
EPSCs
IPSCs
Response Latency (ms)
i
n
control
+ NBQX & APV
+ SR & CGP
10 pA
p
+ TTX & 4AP
q
5 ms light pulses
0.5 ms light pulses
light-evoked EPSC amplitude (pA)
Time (min)
j
o
Amplitude (pA)

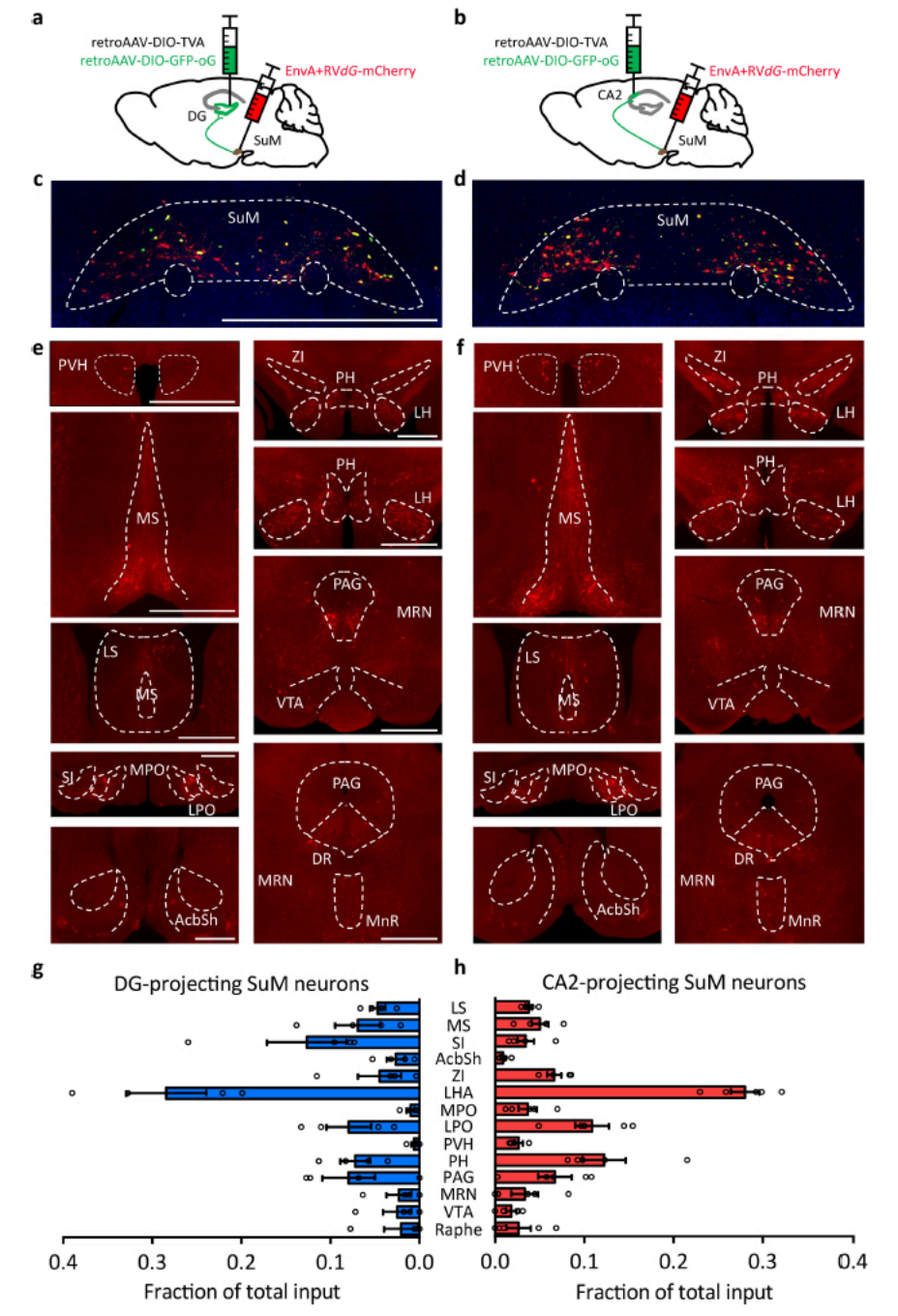
a
retroAAV-DIO-TVA
retroAAV-DIO-GFP-oG
EnvA+RV*dG*-mCherry
DG
SuM
b
retroAAV-DIO-TVA
retroAAV-DIO-GFP-oG
EnvA+RV*dG*-mCherry
CA2
SuM
c
SuM
d
SuM
e
PVH
ZI
PH
LH
MS
PH
LH
PAG
MRN
LS
MS
VTA
SI
MPO
LPO
PAG
DR
MRN
AcbSh
MnR
f
PVH
ZI
PH
LH
MS
PH
LH
PAG
MRN
LS
MS
VTA
SI
MPO
LPO
PAG
DR
MRN
AcbSh
MnR
g
DG-projecting SuM neurons
LS
MS
SI
AcbSh
ZI
LHA
MPO
LPO
PVH
PH
PAG
MRN
VTA
Raphe
0.4
0.3
0.2
0.1
0.0
Fraction of total input
h
CA2-projecting SuM neurons
0.0
0.1
0.2
0.3
0.4
Fraction of total input